Reviewed Preprint
v1 • November 19, 2024
Not revised

Reviewed Preprint
v2 • June 16, 2026
Revised by authors

The chromokinesin Kid (KIF22) forms a homodimer, moves processively along microtubules and transports double-stranded DNA

Shinsuke Niwa[1,2,*], **Natsuki Furusaki**[2,*], **Tomoki Kita**[2], **Yuki Suzuki**[3], **Kyoko Chiba**[1]

[1]Frontier Research Institute for Interdisciplinary Sciences (FRIS), Tohoku University, Sendai, Japan • [2]Graduate School of Life Sciences, Tohoku University, Sendai, Japan • [3]Mie University, Graduate School of Engineering, Tsu, Japan

For correspondence:
shinsuke.niwa.c8@tohoku.ac.jp
kyoko.chiba.e7@tohoku.ac.jp

* These authors equally contributed to this work

Competing interests: No competing interests declared

Funding: See page 19

Reviewing editor: Kassandra M Ori-McKenney, University of California, United States

eLife Assessment

This **important** study clarifies the mechanism by which the kinesin-10 motor protein, chromosome-associated kinesin, Kid (KIF22), enables chromosome movement during mitosis, demonstrating that human and Xenopus Kid proteins function as processive, homodimeric kinesins capable of processive microtubule plus-end motility. The **convincing** work highlights that Kid can recruit and transport duplex DNA along microtubules via its conserved C-terminal DNA binding domain, revising our understanding of chromokinesins' role in chromosome motility during mitosis. It will be of interest to those in the molecule motor community working at the molecular, cellular, and organismal levels.

https://doi.org/10.7554/eLife.102828.2.sa3

Abstract

During prometaphase in mitosis, chromosomes are pushed toward the spindle equator. The chromokinesin Kid, also known as KIF22, moves chromosomes along spindle microtubules during prometaphase. Kid has long been considered a monomeric and non-processive motor, different from typical kinesins. In this study, we demonstrate that the full-length Kid forms a homodimer and moves processively along microtubules. A conserved coiled-coil domain within the stalk region of Kid is sufficient for homodimer formation and is required for the processivity of Kid. Furthermore, the neck linker and coiled-coil domains of Kid could add processive activity to the motor domain of KIF1A, suggesting that Kid contains a functional neck linker and dimerization capability, a prerequisite for the processivity of kinesin motor domains. The full-length Kid, containing a helix-hairpin-helix domain, can transport double-stranded DNA along microtubules in vitro. Alphafold3 prediction suggests that the dimerization of Kid stabilizes the association with DNA. These findings collectively suggest the reclassification of Kid as a processive and dimeric motor that transports DNA along microtubules.

Introduction

Microtubules are reorganized to form a bipolar spindle as cells enter mitosis. In the prometaphase of mitosis, chromosomes are transported along the microtubules toward the spindle equator (Rieder et al., 1986). This process, known as chromosome congression, requires kinesin-4, kinesin-10 and kinesin-12 class of motor proteins (Bieling et al., 2010; Iemura and Tanaka, 2015; Wordeman, 2010). The mechanical forces that move chromosomes toward the spindle equator is called polar ejection forces (Brouhard and Hunt, 2005; Levesque and Compton, 2001; Rieder et al., 1986). The Kinesin-like DNA-binding protein (Kid), belonging to the kinesin-10 family and also known as KIF22, serves as a main molecular motor that transports

chromosomes and generates polar ejection forces (Brouhard and Hunt, 2005; Levesque and Compton, 2001; Ohsugi et al., 2003; Thompson et al., 2022; Tokai et al., 1996; Wandke et al., 2012). Structurally, Kid contains a kinesin motor domain (Yajima et al., 2003), a coiled-coil domain (Shiroguchi et al., 2003), and a DNA binding domain (Tokai et al., 1996) (Figure 1A). In mitosis, the DNA binding domain of Kid binds along chromosome arms (Antonio et al., 2000; Funabiki and Murray, 2000; Levesque and Compton, 2001). Using the motor domain, Kid transports chromosomes (Bieling et al., 2010; Brouhard and Hunt, 2005).

A single kinesin molecule can move for hundreds of steps along a microtubule without dissociating (Hackney, 1995; Hancock and Howard, 1998). This property, called processivity, requires dimerization of kinesins (Hancock and Howard, 1998). However, Kid has long been regarded as a monomeric and non-processive motor, which can move along microtubules in only a single step (Shiroguchi et al., 2003; Yajima et al., 2003). Consistent with these findings, Kid is unique within kinesin superfamily due to lack of the conventional neck coiled-coil domain (Shiroguchi et al., 2003), an element that determines the length of the neck linker essential for the coordinated movement of the two motor domains (Case et al., 2000; Isojima et al., 2010; Yildiz et al., 2008). On the other hand, a previous study showed that the coiled-coil domain of Kid interacts with full-length Kid in GST pull-down assays, suggesting this domain may mediate dimerization of Kid (Pike et al., 2018). In addition, full-length human Kid was reported to move processively along microtubules (Stumpff et al., 2012) and, Kid was proposed to be a chemically processive motor (Walker et al., 2019). However, these studies did not show the oligomeric state of Kid, nor did they provide detailed information on its motility characteristics and parameters. A Drosophila kinesin-10 motor NOD, an orthologue of Kid, is also characterized as a monomeric and non-processive motor (Matthies et al., 2001). Similar to Kid, NOD has a DNA binding domain at the tail domain (Afshar et al., 1995). NOD shows a processive movement only when the protein is forcedly dimerized by the addition of an artificial coiled-coil domain (Ye et al., 2018). Nevertheless, Kid acts as an active motor in microtubule gliding assays and cargo transport assays, both of which detect movement generated by multiple Kid motors (Bieling et al., 2010; Li et al., 2016; Shiroguchi et al., 2003; Takagi et al., 2013). Collectively, it has been widely assumed that Kid, unlike other kinesins, transports chromosomes by their cooperative action of many non-processive monomers (Brouhard and Hunt, 2005; Iemura and Tanaka, 2015; Takagi et al., 2013; Thompson et al., 2022).

Recently, we and others have analyzed properties of full-length kinesins (Chiba et al., 2022; Chiba et al., 2019; Fan, 2022; Wang et al., 2022). Notably, these studied have found that monomeric kinesins, including KIF1A, UNC-104 and KIF13B are converted to a dimer when activated (Chiba et al., 2023; Fan, 2022; Kita et al., 2024; Tomishige et al., 2002). For instance, in the autoinhibited and inactive state, KIF1A and UNC-104 are monomeric (Kita et al., 2024; Tomishige et al., 2002). The monomeric motor domain of UNC-104 and KIF1A has a plus-end directed motor activity but exhibits one-dimensional diffusion, meaning that the efficiency is low (Okada et al., 2003; Tomishige et al., 2002). Upon the release of autoinhibition, KIF1A and UNC-104 form dimers, which exhibit efficient directional movement on microtubules (Kita et al., 2024). These studies prompted us to reanalyze the oligomeric state and the motile properties of Kid, mainly in the full length. In this study, we show that the full-length Kid protein moves processively along microtubules. Kid proteins can form dimers but Kid proteins are dissociated to monomers at low concentrations. In the reconstitution assays in vitro, full-length Kid transport double-stranded DNA along microtubules.

Results

Kid exhibits processive movement along microtubules

To study biochemical and biophysical properties of full-length Kid, we firstly purified the full-length human Kid (hKid) and Xenopus Kid (XKid) using the baculovirus system and Sf9 cells because a previous study has succeeded in purifying functional XKid from Sf9 cells (Bieling et al., 2010; Funabiki and Murray, 2000; Takagi et al., 2013). hKid as well as XKid possesses an N-

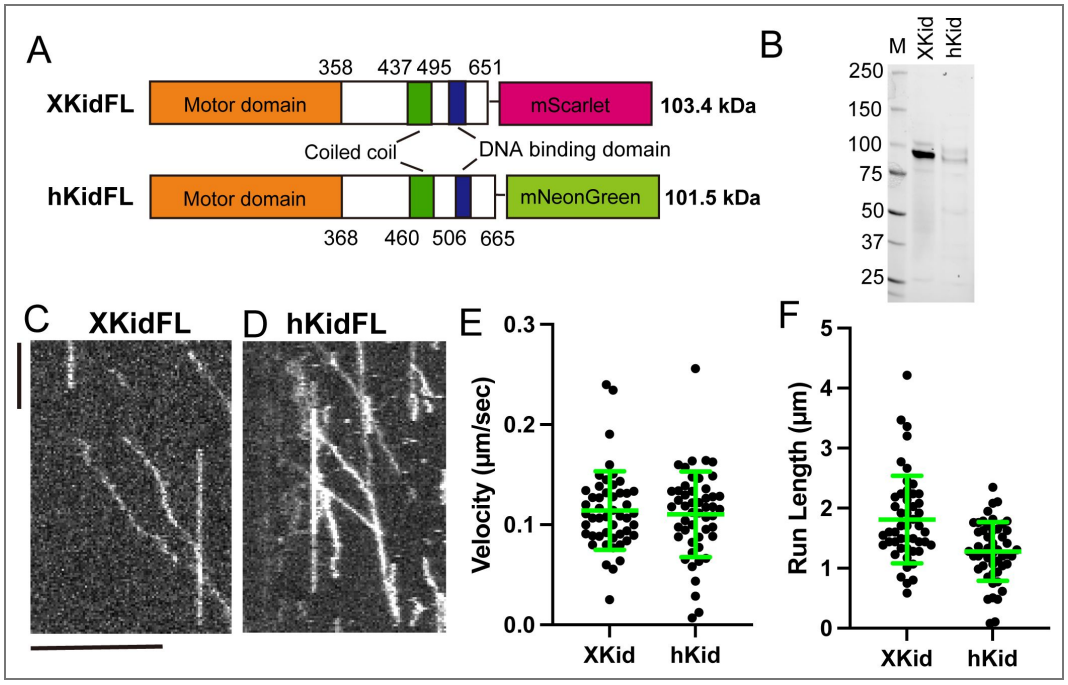

Figure 1. **Kid is a processive motor**

(A) Schematic illustration of the domain organization in Xenopus Kid tagged with a fluorescent protein mScarlet (XKidFL) and human Kid tagged with mNeonGreen (hKidFL). The calculated molecular weights of the fusion proteins are indicated on the right. (B) Representative SDS-PAGE analysis of purified XKidFL and hKidFL fusion proteins. The proteins are visualized using a Stain-Free gel. The molecular weight standards are indicated on the left side of the SDS-PAGE images. (C and D) Representative kymographs showing the motility of XKidFL at 20 pM (C) and hKidFL at 20 pM (D) both in the presence of 2 mM ATP. Scale bars: horizontal, 10 µm; vertical, 60 seconds. (E) Dot plots showing the velocity of XKidFL and hKidFL. Each dot shows a single datum point. Green bars represent mean ± S.D.. n = 51 and 52, respectively. (F) Dot plots showing the run length of XKidFL and hKidFL. Each dot shows a single datum point. Green bars represent mean ± S.D.. n = 51 and 52, respectively.

terminal motor domain, a short coiled-coil domain and a DNA binding tail domain (Figure 1A). Previous studies have shown that hKid and XKid, that are fused with fluorescent proteins at the C-terminal, can complement the function of hKid-depleted cells and XKid-depleted Xenopus egg extracts (Bieling et al., 2010; Soeda et al., 2016). Thus, we fused a fluorescent protein at the C-terminal of XKid and hKid. Notably, while EGFP-fused and sfGFP-fused hKid were insoluble, mNeonGreen-fused hKid was recovered from soluble fractions. As a result, we succeeded in purifying both XKid-mScarlet and hKid-mNeonGreen proteins (Figure 1B, and supplemental Figure S1). Next, the motility of purified proteins were analyzed by single molecule motility assays using total internal reflection fluorescent microscopy (TIRF). We found that both XKid and hKid moved on microtubules processively (Figure 1C, D, Movie 1 and 2). The motility of single molecules along microtubules could be observed at 20 pM of Xkid and hKid, respectively. The average velocity of XKid and hKid were approximately 110 nm/sec (Figure 1E and Table 1), within the same range as the movement of chromosomes (Brouhard and Hunt, 2005). The run length of XKid and hKid were 1.8 ± 0.7 and 1.3 ± 0.5 μm, respectively (Figure 1F and Table 1). These data collectively suggest that full-length Kid is a processive motor protein.

Full-length Kid form dimers

It has been proposed that Kid is a monomeric protein (Shiroguchi et al., 2003; Yajima et al., 2003). Even full-length human Kid protein obtained from 293T cells are indicated to be a monomer (Shiroguchi et al., 2003). However, typical kinesins show processive movement along microtubules only when they form dimers (Hancock and Howard, 1998; Kita et al., 2024; Tomishige et al., 2002). As both hKid and XKid showed processive movement on microtubules (Fig 1), we next analyzed the oligomeric state of these motors using size exclusion chromatography (Fig 2A and B). We utilized the previously well-characterized kinesin UNC-104(1-653)-sfGFP as a size marker. UNC-104(1-653)-sfGFP exhibits a dimer peak at 200 kDa and a monomer peak at 100 kDa in size exclusion chromatography (Kita et al., 2024). This characteristic makes it a suitable marker for determining the oligomeric state of hKid and XKid, given that the predicted molecular weights of hKid-mNeonGreen and XKid-mScarlet monomers are approximately 100 kDa (Figure 1A). As a result, we found that the peak fraction of full-length hKid and XKid are almost equivalent to that of UNC-104(1-653)-sfGFP dimer (Fig 2A and B, and supplemental Figure S2). Notably, unlike UNC-104(1-653)-sfGFP, we did not detect any monomer peaks for hKid and XKid under these conditions. We next analyzed purified proteins recovered from the peak fractions using mass photometry (Sonn-Segev et al., 2020). Mass photometry is generally performed at the nanomolar concentrations (Sonn-Segev et al., 2020). Peak fractions obtained from size exclusion chromatography were diluted 100-fold and analyzed by mass photometry. Mass photometry analysis revealed a predominant monomer population, with a smaller fraction corresponding to dimers (Figure 2C and D). The behavior is similar to that of UNC-104(1-653)-sfGFP, which shows dimer peaks by size-exclusion chromatography at micromolar concentrations but dissociates into monomers at the nanomolar concentrations used for mass photometry (Kita et al., 2024). In addition, we consistently detected a minor trimer populations under this condition (Figure 2C and D), although this species may represent an artifact because it was not detected by size-exclusion chromatography. These findings indicate that full-length hKid and XKid are capable of forming dimers, but the dimer formation is dependent on the protein concentration.

A conserved coiled-coil domain is essential for the processivity

Table 1. **Motile properties of constructs used in this study**

Motor protein constructs underwent purification through affinity chromatography followed by size exclusion chromatography, as detailed in the Materials and Methods section. The reported velocities and run lengths represent mean values ± standard deviation (SD). Notably, XKid(1-437) failed to demonstrate consistent processive motion across three separate protein preparations, indicating a lack of detectable activity (ND: not detected).

	Processive	Oligomeric state in SEC	Velocity (μm/sec)	Run length (μm)
Full length hKid	Yes	Dimer	0.11 ± 0.04	1.8 ± 0.7
Full length XKid	Yes	Dimer	0.11 ± 0.04	1.3 ± 0.5
XKid(1-496)	Yes	Dimer	0.12 ± 0.03	3.1 ± 2.4
XKid(1-437)	No	Monomer	nd	nd
KIF1A(1-393)LZ	Yes	Dimer	1.4 ± 0.4	11 ± 11
KIF1AMD-XKidSt	Yes	Dimer	0.67 ± 0.18	6.7 ± 6.0

Figure 2. **Kid forms a weak dimer**

(A) Size exclusion chromatography profiles of hKidFL (black) and UNC-104(1-653)-sfGFP (cyan). Below the chromatography, an SDS-PAGE image show the elution fractions. Asterisks indicate fractions used for mass photometry and single molecule assays. The molecular weight standards are indicated on the left side of the SDS-PAGE images. (B) Size exclusion chromatography of XKidFL (black) and UNC-104(1-653) (cyan). The SDS-PAGE of the elution fractions are shown beneath the profiles. Asterisks indicate fractions used for mass photometry and single molecule assays. The number shown at the left side indicates molecular weight standard. (C) Mass photometry analysis of human Kid at 10 nM. Histograms show particle counts, and lines indicate Gaussian fits. The mean ± SD and percentage of each peak are shown. (D) Mass photometry analysis of human Kid at 10 nM. Histograms show particle counts, and lines indicate Gaussian fits. The mean ± SD and percentage of each peak are shown. Note that majority of hKid and XKid are dimers in the size exclusion chromatography but they are mostly dissociated to monomers in mass photometry.

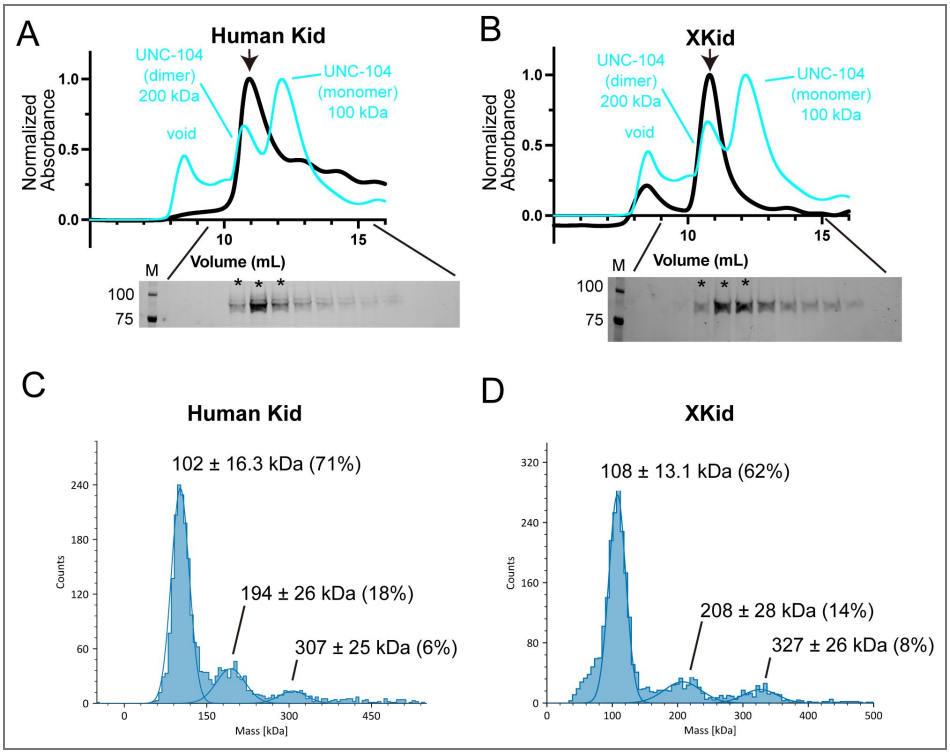

To determine the domain essential for the processive movement of Kid, we generated a series of deletion mutants. Unfortunately, we failed to purify adequate quantities and qualities of hKid deletion mutants. Thus, following experiments were performed using XKid. We purified XKid(1-496), which lacks the DNA-binding tail domain, and XKid(1-437), which lacks the DNA-binding domain and the coiled-coil domain (Figure 3A and B, and supplemental Figure S1). Mass photometry showed that XKid(1-496) was predominantly monomeric (Fig 3C), with minor dimer and trimer populations, resembling the behavior of full length XKid (Figure 2). In contrast, XKid(1-437) was exclusively monomeric (Fig 3D).

Using these purified proteins, we performed single molecule motility assays (Fig 3E-H). We found XKid(1-496) could move processively on microtubules (Fig 3E). The velocity of XKid(1-496) was approximately 120 nm/sec and the run length was 3.1 ± 2.4 μm, which are comparable to those of full-length XKid (Table 1). Thus, DNA binding domain of Kid is not required for processive runs. In contrast, XKid(1-437), which lacks the coiled-coil domain, did not show any processive runs (Fig 3F). To analyze the motile properties, we performed the mean square displacement (MSD) analysis (Fig 3 G and H). The MSD curves were fitted to the power-law relationship $MSD = A(\Delta t)^{\alpha}$, where α describes how the displacement scales with time. α = 1 indicates simple diffusion, α > 1 indicates superlinear MSD scaling indicating persistent or directionally biased motion, and α < 1 indicates sublinear MSD scaling indicating constrained motion. XKid(1–496) had an α value of approximately 1.6, consistent with directionally biased movement, whereas XKid(1–437) had an α value of approximately 0.8, indicating sublinear MSD scaling consistent with hindered motion (Figs. 3G 3H). This would be because XKid(1-437) did not form a homodimer, considering that coiled-coil domains are generally required for the dimerization of kinesins (Hancock and Howard, 1998; Kita et al., 2024).

To confirm that the coiled-coil domain of XKid induces dimerization, the domain was fused with mScarlet and analyzed by the size exclusion chromatography (Fig 3I and J). As a result, the peak of XKidCC-mScarlet shifted to the larger size compared with that of mScarlet. The calculated molecular weight of XKidCC-mScarlet was 42 kDa, which is almost equivalent to the size of dimerized mScarlet. To test whether monomeric Kid molecules in solution form dimers on microtubules, hKid-mScarlet3 and hKid-mStayGold were purified separately, mixed at final concentrations of 1 pM each, and analyzed using single-molecule motility assays (Fig 4). Under these assay conditions, hKid is expected to be monomeric in solution, because mass photometry showed that hKid was predominantly monomeric even at a much higher concentration of 10 nM (Figure 2). As a result, approximately 20% of motile hKid-mScarlet3 particles showed comigration with hKid-mStayGold particles along microtubules, suggesting microtubule-dependent association between hKid molecules.

The stalk domain of XKid adds processivity to the motor domain of KIF1A

In the processive movement along the microtubules, the coordination between two motor domains is essential (Hancock and Howard, 1998). The neck linker domain, immediately following the kinesin motor domain, regulates the ATPase activity within the motor domain (Case et al., 2000). It has been shown that optimal length of the neck linker domain is crucial for achieving coordination of the two motor domains (Isojima et al., 2010; Yildiz et al., 2008). The length of the neck linker domain is typically determined by the presence of the neck coiled-coil domain (Case et al., 2000; Shastry and Hancock, 2010). However, Kid is an exception, as it does not have the conventional neck coiled-coil domain (Shiroguchi et al., 2003; Tokai et al., 1996). This unique feature of Kid supports the idea that Kid functions as a non-processive monomer (Yajima et al., 2003), which does not require the coordination between two motor domains. However, coiled-coil prediction tools might not identify hidden coiled-coil domains or Kid could have a motif that induces dimerization. In the case of kinesin-1, Alphafold2, but not coiled-coil prediction tools, can more accurately find the location of coiled-coil domains (Tan et al., 2023; Weijman et al., 2022). Therefore, we used Alphafold2 to analyze the neck-linker and the first coiled-coil domain of XKid and hKid. The regions corresponding to residues 359–495 of XKid

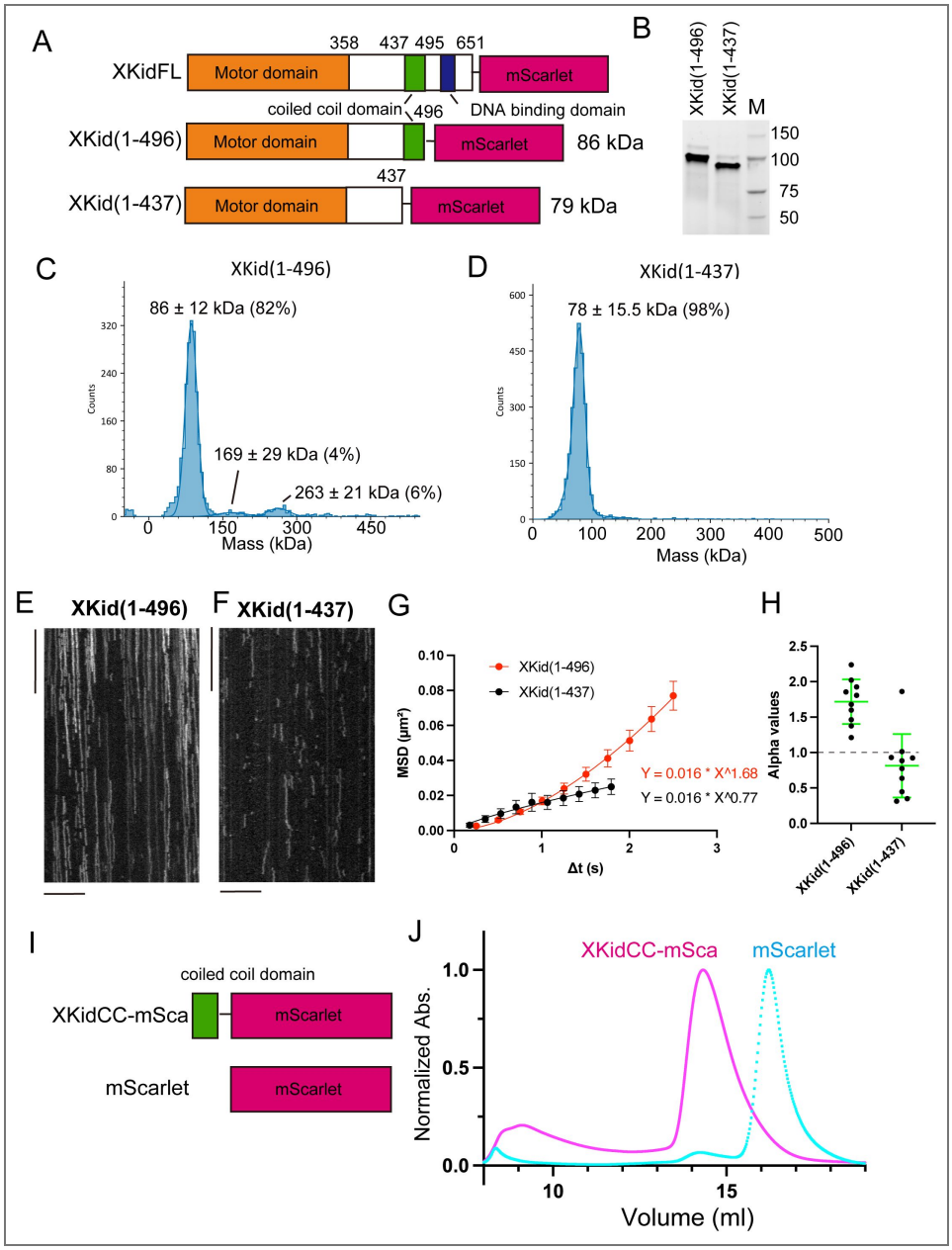

Figure 3. Conserved coiled-coil domain is required for the processive motion

(A) Schematic representation illustrating the domain organization of XKid(1-496) and XKid(1-437). The calculated molecular weights of the fusion proteins are indicated on the right. (B) Representative SDS-PAGE analysis of purified XKid(1-496) and XKid(1-437) proteins. The proteins are visualized using a Stain-Free gel. The molecular weight standards are indicated on the right side of the SDS-PAGE images. (C and D) Mass photometry analysis of XKid(1–496)-mSca and XKid(1–437)-mSca. The expected molecular masses are 86 and 79 kDa, respectively. Histograms show particle counts, and lines indicate Gaussian fits. The mean ± SD and percentage of total counts for each peak are shown. (E and F) Representative kymographs showing the motility of 10 pM XKid(1-496) (E) and XKid(1-437) (F) in the presence of 2 mM ATP. Note that no directional movement was detected in XKid(1-437). Scale bars: horizontal 10 μm; vertical 10 seconds. (G and H) Mean-square displacement (MSD) analysis of XKid(1–496) and XKid(1–437) trajectories. (G) Representative MSD curves fitted to the power-law relationship MSD = $A\Delta t^{\alpha}$, where α is the anomalous diffusion exponent. XKid(1–496) showed superlinear MSD scaling with α = 1.68, consistent with persistent or directionally biased motion, whereas XKid(1–437) showed sublinear MSD scaling with α = 0.77. (H) Distribution of α values obtained from individual trajectory fits. Each dot represents one trajectory; bars indicate mean ± SD. n = 10 trajectories per construct. (I and J) Schematic drawing of XKidCC-mScarlet (I) and a representative result of size exclusion chromatography (J). XKidCC-mScarlet (magenta) and mScarlet (cyan) are shown.

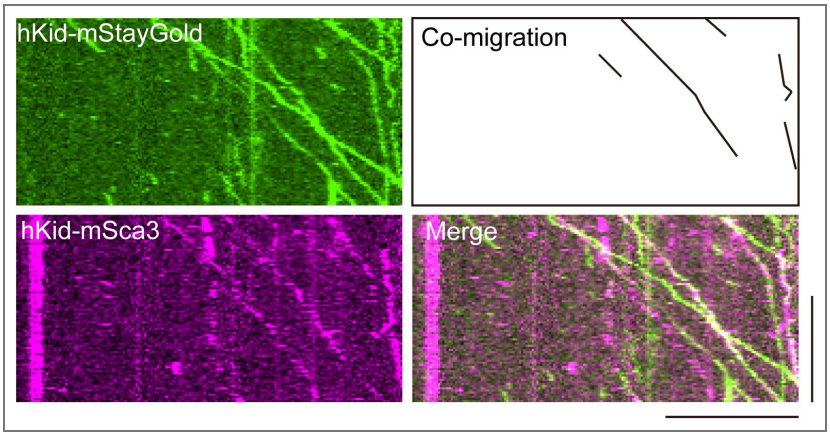

Figure 4. Human Kid–mStayGold and Kid–mScarlet3 co-migrate on microtubules.

Purified hKid–mStayGold and hKid–mScarlet3 were mixed at final concentrations of 20 pM each and analyzed by single-molecule motility assays using TIRF microscopy. Representative kymographs show hKid–mStayGold, hKid–mScarlet3, and merged signals. The schematic drawing illustrates examples of co-migrating particles on microtubules, defined as overlapping mStayGold and mScarlet3 signals moving together along the same microtubule. Co-migration was defined as overlapping mStayGold and mScarlet3 signals moving together along the same microtubule over the same time interval. Scale bars: horizontal, 10 μm; vertical, 100 s.

and 369–506 of hKid were modeled using AlphaFold 2 (Figure 1A). The result suggested that the region does not have hidden coiled-coil domains nor a motif that induces dimerization, and the region is flexible (Supplementary Figure S3). If the entire flexible region functions as a neck linker, its length is 4 times longer than that of kinesin-1 (Supplementary Figure S3). To investigate if this extended neck linker of Kid can support the coordination of two motor domains, we fused the coiled-coil domain of XKid to the motor domain of KIF1A (Figure 5A). We included the possible neck linker domain of XKid in this chimera protein to test whether the neck linker of XKid is functional or not (Figure 5B). We could purify the chimeric protein, named KIF1AMD-XKidSt (Figure 5C and supplementary Figure S1). We found that KIF1AMD-XKidSt exhibited processive movement along microtubules in the single molecule motility assay (Figure 5D and movie S3), as is the case of KIF1A(1-393)LZ (Figure 5E and movie S4). The velocity of KIF1AMD-XKidSt was much faster than original XKid but slightly slower than KIF1A(1-393)LZ (Figure 5F and Table 1). The run length of KIF1AMD-XKidSt was shorter than KIF1A(1-393)LZ (Figure 5G and Table 1). Previous studies have shown that the motor domain of KIF1A does not exhibit processive motion when it is monomeric, but exhibits processive motion when an artificial dimer is generated using a stalk domain of kinesin-1 or a leucine zipper domain (Soppina et al., 2014; Tomishige et al., 2002). Therefore, these results suggest that the coiled-coil domain of XKid can induce dimerization of KIF1A motor domains on microtubules and the longer neck linker domain of XKid can support the processive movement of the kinesin motor domain.

Reconstitution of DNA transport in vitro

Kid was originally identified as a DNA binding protein (Tokai et al., 1996). The tail domain of Kid has two helix-hairpin-helix motif which is supposed to be a DNA binding domain (Doherty et al., 1996). To test that Kid has an activity to transport DNA along microtubules, we mixed fluorescently-labelled DNA in TIRF assays and directly observed the motility (Figs 6A-D). To study the domains essential for the transport of DNA, we used full-length XKid and a deletion mutant of Xkid for these assays. We found that full-length XKid can drive the movement of double-stranded DNA along microtubules (Fig. 6A). Double-stranded DNA signals that co-migrated with XKid were 93.4 ± 10.5 % (n = 31 microtubules). The velocity of double-stranded DNA moving along microtubules was approximately 100 nm/sec, which is similar to the velocity of XKid alone (Figure 1). In contrast, single-strand DNA movement was not driven by XKid (Fig. 6B and D). Deletion of the tail domain of XKid, containing helix-hairpin-helix motif, abolished the DNA transport activity (Fig 6C and D). We confirmed that full-length hKid can also induce the movement of double-stranded DNA along microtubules (Figure S4 and supplemental movie S5).

Next, we analyzed dsDNA fragments of different lengths. Full-length Kid transported not only 100-bp dsDNA but also longer 1,000-bp and 2,000-bp dsDNA fragments along microtubules (Fig. 6E-G). However, the velocity and run length of DNA transport were comparable among these substrates (Fig. 6H and I), suggesting that increasing DNA length does not substantially alter Kid-driven DNA transport under our reconstituted assay conditions.

Dimerization would be required for DNA transport

The structure of the XKid–DNA complex was modeled using AlphaFold3 (Fig 7A-D). We first modeled one copy of the DNA-binding domain of XKid with a 15-bp DNA fragment (Fig 7A). This prediction yielded low ipTM and pTM values of 0.12 and 0.64, respectively, and did not produce a clear XKid-DNA complex model. We then modeled two copies of the DNA-binding domain of XKid with a double-stranded DNA fragment (Figure 7B–D). In this case, AlphaFold 3 generated a model in which two DNA-binding domain of XKid associate with dsDNA. The ipTM and pTM values were 0.79 and 0.84, respectively, suggesting a higher-confidence prediction of the complex. To further examine whether the DNA-binding domain of XKid intrinsically forms a stable dimer, we performed AlphaFold3 prediction in the absence of DNA. This prediction yielded only modest confidence scores (ipTM = 0.34, pTM = 0.57). These results suggest that the dimeric configuration of the DNA-binding domain of XKid is preferentially stabilized in the presence of double-stranded

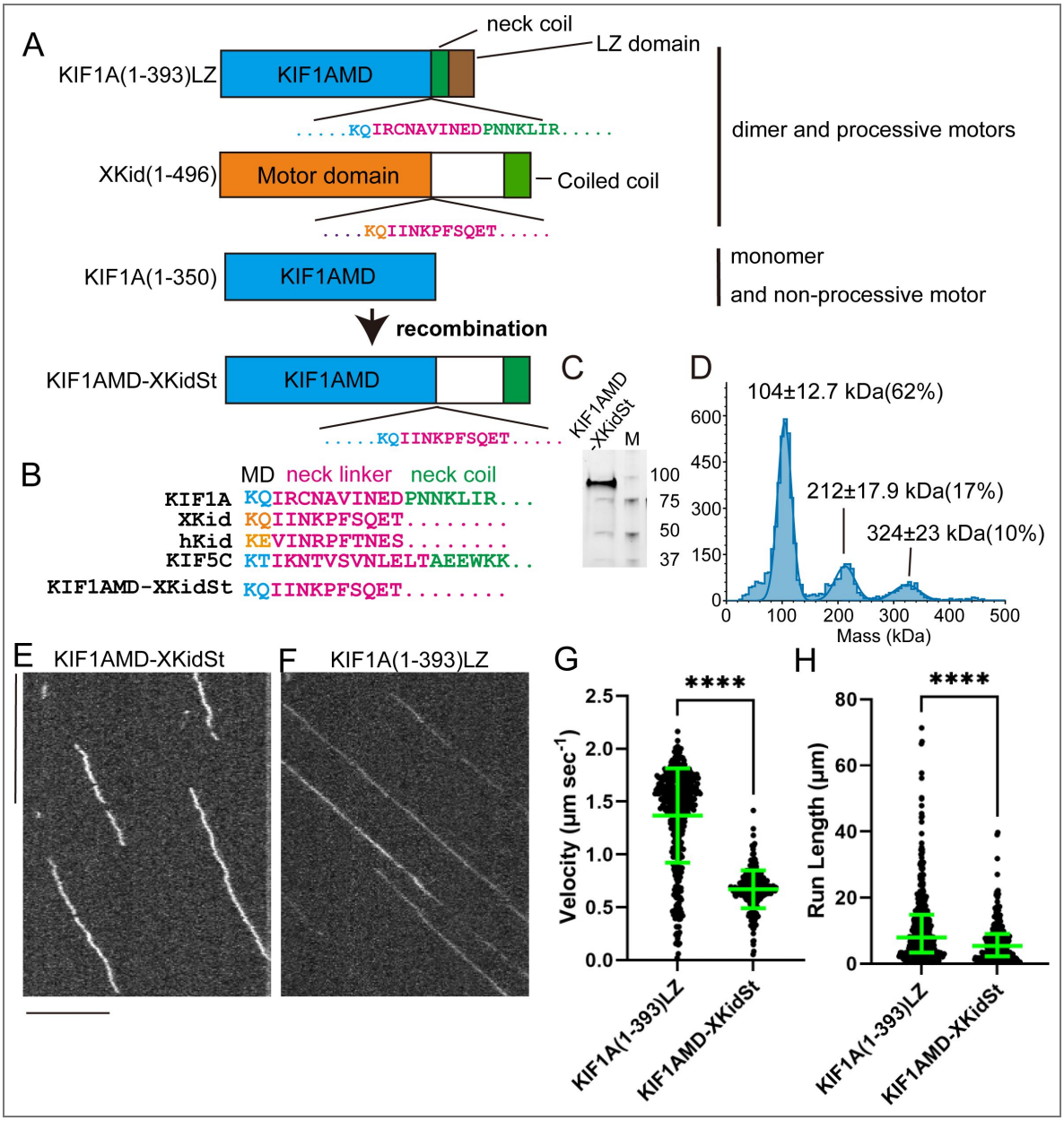

Figure 5. Untypical neck linker of Kid can support processive movement of KIF1A

(A) Schematic representation illustrating the domain organization of KIF1A(1-393)LZ, XKid(1-496), KIF1A(1-350) and a chimera protein KIF1AMD-XKidSt. Note that KIF1A(1-393)LZ and XKid(1-496) are processive motors and KIF1A(1-350) is a non-processive motor. Cyan, motor domain of KIF1A; Orange, motor domain of Kid; Magenta, neck linker. (B) Amino acid sequences of the neck linker region. KIF1A, XKid, hKid, KIF5C and KIF1AMD-XKidSt are shown. Cyan, motor domain of KIF1A and KIF5C; Orange, motor domain of Kid; Magenta, neck linker; Green, neck coiled-coil domain. (C) Representative SDS-PAGE analysis of purified KIF1AMD-XKidSt fusion protein. The protein is visualized using a Stain-Free gel. The molecular weight standards are indicated on the right side of the SDS-PAGE image. (D and E) Representative kymographs showing the motility of KIF1AMD-XKidSt and KIF1A(1-393)LZ in the presence of 2 mM ATP. Note that KIF1AMD-XKidSt exhibits diffusion-like fluctuations while they are moving. This phenomena is not observed in KIF1A(1-393)LZ. Scale bars: horizontal 10 μm; vertical 10 seconds. (F) Dot plots showing the velocity of KIF1AMD-XKidSt and KIF1A(1-393)LZ. Each dot shows a single datum point. Green bars represent mean ± S.D.. ****, $p < 0.0001$, Unpaired t-test. n = 273 and 434 particles for KIF1AMD-XKidSt and KIF1A(1-393)LZ, respectively. (G) Dot plots showing the run length of KIF1AMD-XKidSt and KIF1A(1-393)LZ. Each dot shows a single datum point. Green bars represent median value and interquartile range. ****, $p < 0.0001$, Mann-Whitney test. n = 273 and 434 particles for KIF1AMD-XKidSt and KIF1A(1-393)LZ, respectively.

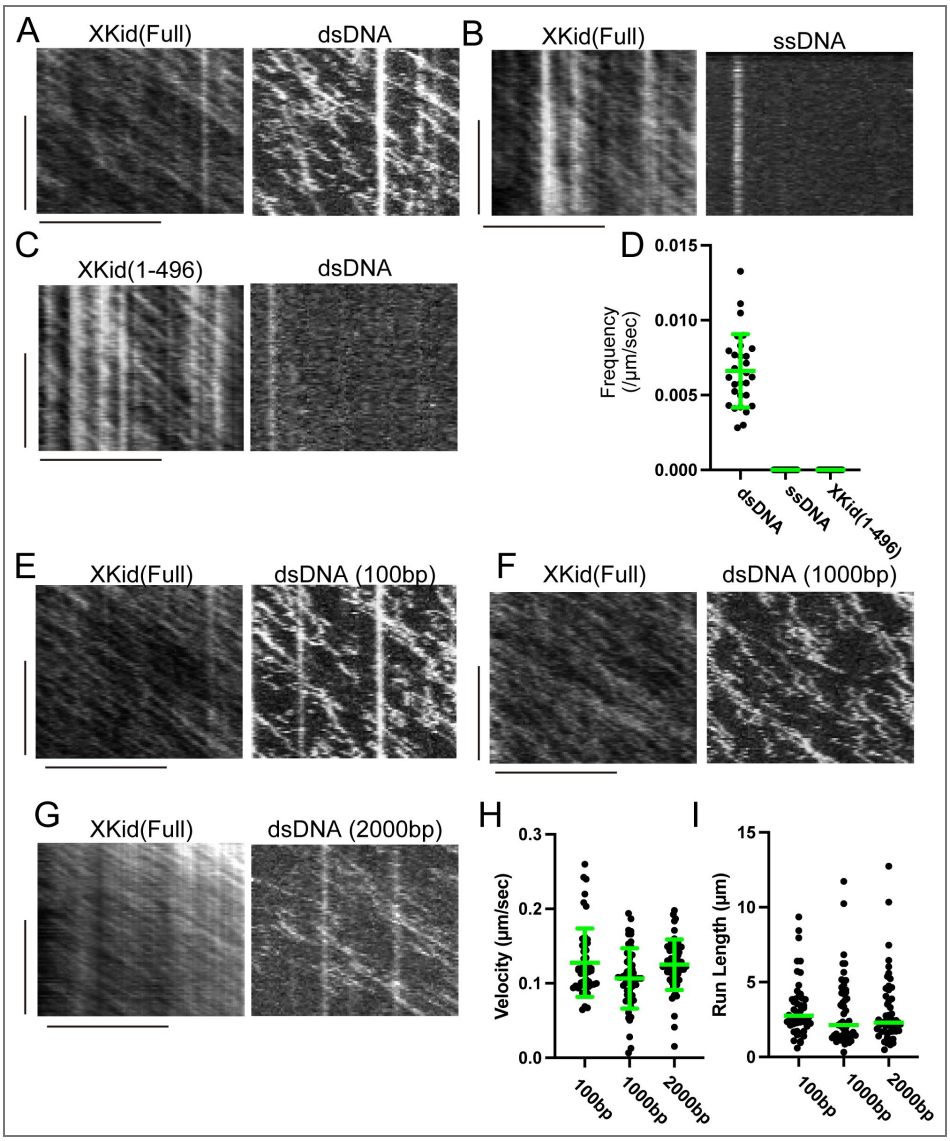

Figure 6. **DNA movement driven by XKid**

(A–D) sfGFP-tagged XKid at 1 nM was mixed with 20 nM Cy3-labeled double-stranded or single-stranded DNA and observed by TIRF microscopy. (A–C) Representative kymographs showing the movement of full-length XKid with double-stranded 100-bp DNA (A), full-length XKid with single-stranded 100-base DNA (B), and XKid(1–496) with double-stranded 100-bp DNA (C). Scale bars: horizontal, 10 μm; vertical, 100 s. (D) Frequency of DNA movement along microtubules, normalized by microtubule length and observation time. Each dot represents an individual measurement from a different microtubule. Bars indicate mean ± SD. n = 29 microtubules per condition. (E–I) Single-molecule analysis of XKid–sfGFP on Cy3-labeled DNA. Purified XKid–sfGFP was mixed with Cy3-labeled DNA at final concentrations of 1 nM XKid–sfGFP and 20 nM DNA and observed by TIRF microscopy. (E–G) Representative kymographs showing the movement of full-length XKid–sfGFP on 100-bp DNA (E), 1000-bp DNA (13 ng/μl; F), and 2000-bp DNA (26 ng/μl; G). Scale bars: horizontal, 10 μm; vertical, 100 s. (H) Velocity of DNA movement along microtubules. Each dot represents one DNA molecule. Bars indicate mean ± SD. n = 48, 53, and 53 DNA molecules for 100-, 1000-, and 2000-bp DNA, respectively. (I) Run length of DNA movement along microtubules. Each dot represents one DNA molecule. Bars indicate mean ± SD. n = 48, 53, and 53 DNA molecules for 100-, 1000-, and 2000-bp DNA, respectively.

DNA. These results suggest that the DNA-binding domain of XKid adopts a DNA-binding architecture more readily in a dimeric configuration. To experimentally test the predicted model, we introduced the K613A mutation into XKid, as K613 was predicted to be located at the XKid–DNA interface (Fig. 7C), and performed dsDNA motility assays (Fig. 7D,E). The XKid(K613A) mutant failed to drive DNA movement in the reconstitution assay (Fig. 7E).

Discussion

Kid is a processive dimer on microtubules

Prometaphase chromosomes are transported along microtubules by the activity of kinesins (Iemura and Tanaka, 2015; Wordeman, 2010). Kid is the primary kinesin that transports chromosomes along spindle microtubules in prometaphase (Brouhard and Hunt, 2005; Iemura and Tanaka, 2015). Previous biochemical studies reported that purified Kid is monomeric, leading to the concept that Kid is a monomeric and non-processive chromokinesin (Yajima et al., 2003; Shiroguchi et al., 2003). Under this model, sustained chromosome movement would require many Kid monomers distributed along chromosome arms to act collectively. Our findings revise this view. Our data show that full-length Kid is capable to form a dimer and exhibits a processive motion along microtubules. In addition, Kid dimers directly bind to dsDNA. Thus, the elementary force-generating unit of Kid is a single Kid dimer which functions as a processive DNA-bound motor. In the context of mitotic chromosomes, multiple processive Kid dimers bound along chromosome arms could cooperate to generate chromosome-scale polar ejection forces (Figure 8). This model preserves the likely importance of motor team on large chromatin. However, the team is likely composed of multiple processive dimers rather than many non-processive monomers.

Biochemical properties of Kid

A notable difference between this study and prior studies is the protein concentration used. Previous analysis of full-length human Kid via density gradient and size exclusion chromatography identified peak fractions through western blot, due to the low concentration of recombinant Kid expressed in 293T cells (Shiroguchi et al., 2003). We show that most hKid and XKid exist as dimers in size exclusion chromatography performed at micromolar concentrations, yet mostly dissociate into monomers in mass photometry, which is performed at nanomolar concentrations (Figure 2). Thus, the inability to detect Kid dimers in earlier studies may be attributed to the low concentration. In mass photometry, we also detected a small population with an apparent trimeric mass (Figs. 2, 3, and 5). Because this species was not detected by size-exclusion chromatography, we interpret this population cautiously and cannot exclude the possibility that it represents a measurement or sample-preparation artifact rather than a stable oligomeric state of Kid. However, transient higher-order oligomerization of Kid in cells, where Kid may be locally concentrated on microtubules or chromatin, remains possible and should be examined in future studies.

Another difference is the methods to detect the processivity of motors. We observed the processivity of Kid by TIRF whereas previous studies observed the motility by optical trap. In optical trapping assays, Kid is diluted prior to being adsorbed onto beads. This dilution likely promotes the dissociation of preformed Kid dimers, consistent with our mass photometry analysis showing that Kid is predominantly monomeric at nanomolar concentrations (Fig. 2), and thus optical trapping assays would primarily monitor monomeric Kid motility. By contrast, in TIRF-based motility assays, Kid in solution binds directly to microtubules. Although Kid is predominantly monomeric in solution, its accumulation on the microtubule surface may increase the local concentration of Kid and promote dimer formation on microtubules. This microtubule-dependent dimerization model could account for the processive motility observed in the TIRF assay. Consistent with this model, when separately purified Kid-mScarlet3 and Kid-mStayGold were mixed, they colocalized and moved processively together along microtubules (Figure 5). However, because of the limited temporal resolution of our two-color imaging system, we could

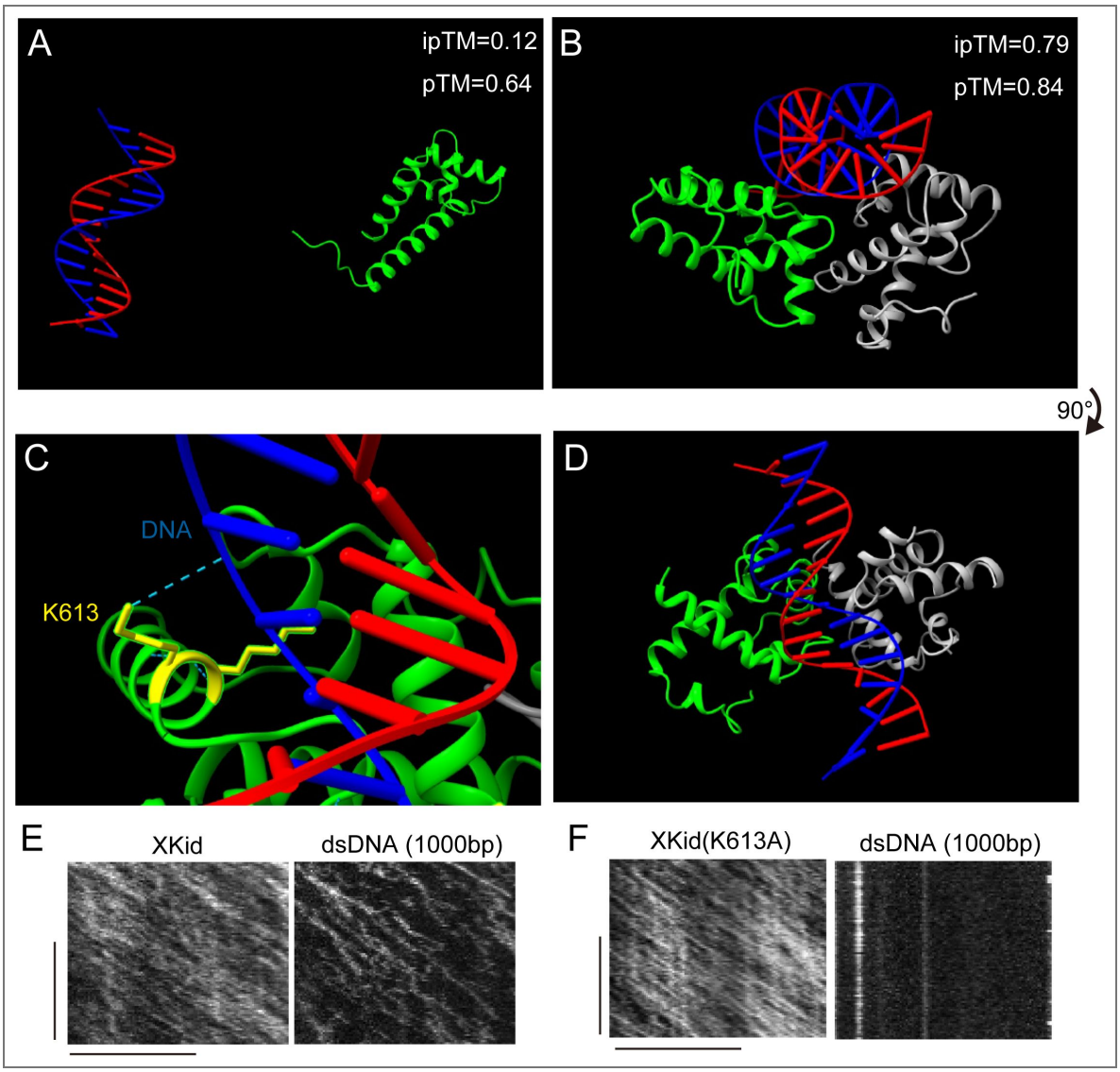

Figure 7. AlphaFold3 prediction and functional validation

(A) AlphaFold3-predicted structure of the XKid DNA-binding domain modeled as a monomer with double-stranded DNA (dsDNA). The prediction showed a low interface confidence score between XKid and dsDNA (ipTM = 0.12, pTM = 0.64). (B–D) AlphaFold3-predicted structure of the XKid DNA-binding domain modeled as a dimer with dsDNA. The two XKid molecules are shown in green and gray, and the two DNA strands are shown in red and blue. This dimeric model showed higher confidence for the XKid–DNA complex (ipTM = 0.79, pTM = 0.84). (B) Side view of the predicted XKid dimer–dsDNA complex. (C) Magnified view of the predicted XKid–DNA interface. K613 and K614, highlighted in yellow, are positioned near dsDNA. A cyan dashed line indicates the predicted hydrogen bond between K613 and DNA. (D) View of the same model shown in (B) after a 90° rotation. (E and F) Representative kymographs showing the movement of dsDNA along microtubules. Wild-type XKid supported movement of 1000-bp dsDNA (E), whereas the K613A mutant abolished detectable dsDNA movement (F). Scale bars: horizontal, 10 μm; vertical, 100 s.

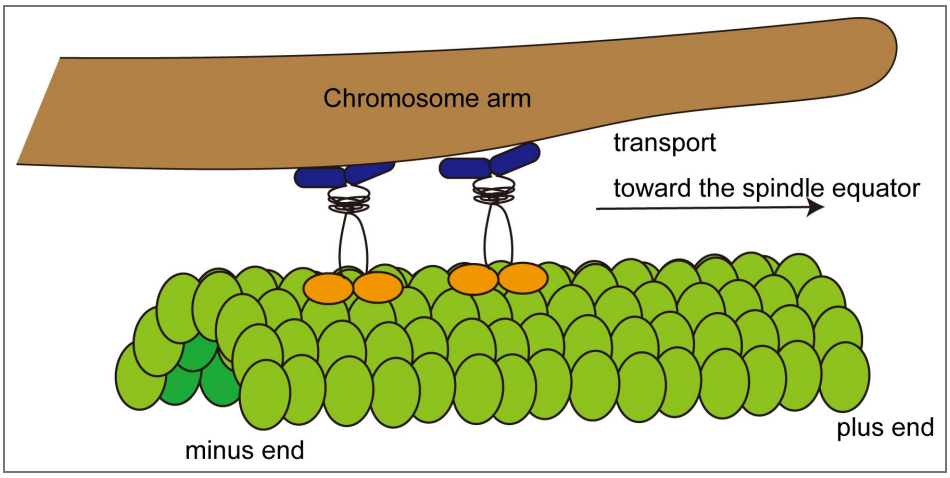

Figure 8. **Model**

Model for Kid-dependent DNA and chromosome transport. Kid forms processive dimers that can directly bind and transport double-stranded DNA along microtubules. On mitotic chromosomes, multiple Kid dimers may bind along chromosome arms and cooperate to generate polar ejection forces. This model is not drawn to scale and does not fully represent the structural complexity of condensed chromatin.

not directly resolve the transition from monomers to dimers on microtubules. These properties, such as “the equilibrium between monomers and dimers” and “the capability to exhibit processive movement on microtubules, even when characterized as monomers through mass photometry” have been observed in kinesin-3 motors (Chiba et al., 2023; Fan, 2022; Kita et al., 2024).

Neck linker of Kid

We show that Kid has a exceptionally long neck linker, approximately four times longer than that of kinesin-1. Neck-linker length strongly influences kinesin processivity, and changes in neck-linker length alter the run length and motility properties of kinesin-1, kinesin-2, and other N-terminal kinesins (Shastry and Hancock, 2010; Shastry and Hancock, 2011). However, longer or non-conventional neck linker regions can also support processive motility and may provide additional functions, such as navigation around microtubule-bound obstacles. Kinesin-2 bypasses Tau and other microtubule-bound obstacles by protofilament switching (Hoeprich et al., 2014). The neck linker of the mitotic kinesin KIF18A contributes to obstacle navigation within the mitotic spindle (Malaby et al., 2019). Thus, the exceptionally long and flexible neck linker of Kid may represent an adaptation that allows this chromokinesin to move processively along crowded spindle microtubules while remaining attached to DNA or chromatin. This possibility remains to be tested directly.

Reconstitution of chromosome congression

A previous in vitro study, using an elegant assay termed chromatin gliding assay, has shown that XKid and XKLP1/KIF4A can crosslink between DNA and microtubules (Bieling et al., 2010). However, it remains to be elusive whether the chromosome transport is mediated by direct binding between chromosomal DNA and motor proteins. In organelle transport, cargo adaptor proteins are generally required for efficient transport (Chiba and Niwa, 2024; Chiba et al., 2022). Our in vitro reconstitution suggests that Kid-dependent chromosome transport does not require cargo adaptor proteins. Rather, our results suggest that dimerization of Kid facilitates DNA binding, allowing Kid to directly couple DNA to microtubule-based motility (Figure 7). Although hKid transported 1,000-bp and 2,000-bp DNA fragments in vitro, their motile parameters were comparable to those of 100-bp DNA. Thus, increasing DNA length did not substantially enhance DNA transport under our reconstituted assay conditions. One possible explanation is that the interaction between Kid and naked DNA is relatively weak or dynamic, and thus only one or a small number of Kid molecules productively engage each DNA molecule during transport. Alternatively, additional Kid molecules bound to longer DNA may not strongly affect the measured motility parameters under these assay conditions. However, naked DNA does not fully recapitulate the structural and mechanical properties of condensed chromatin or mitotic chromosomes. Thus, although multiple Kid dimers may engage chromatin to generate chromosome-scale polar ejection forces, this model remains to be directly tested. Future experiments using chromatinized DNA or reconstituted chromosome-like substrates will be required to determine how Kid interacts with condensed chromatin and how multiple Kid molecules cooperate to move chromosomes during prometaphase.

It has been shown that Kid is regulated by phosphorylation by CDK1(Ohsugi et al., 2003). It would be interesting to study the effects of phosphorylation and dephosphorylation on the Kid-dependent DNA transport using this reconstitution system. Moreover, by extending this system, it may be possible to fully reconstitute the chromosome congression in vitro by including other kinesins and microtubule-associated proteins, such as XKLP1/KIF4A, CENP-E and NuSAP1, that are required for proper chromosome congression (Bieling et al., 2010; Iemura and Tanaka, 2015; Li et al., 2016).

Methods

Plasmids

PCR was performed using a KOD FX neo DNA polymerase (TOYOBO, Tokyo, Japan). Human Kid cDNA (corresponding to DQ895829.2) was described previously (Iemura and Tanaka, 2015). Xenopus Kid (Kif22.S, corresponding to BC070549.1) was purchased from Horizon Discovery. To generate hKidFL-mNeonGreen, DNA fragments encoding human Kid and mNeonGreen were amplified by PCR and assembled into pFastbac1 (Novagen) by Gibson assembly as described (Gibson et al., 2009). To generate XKidFL-mScarlet, DNA fragments encoding XKid and mScarlet were amplified by PCR and assembled into pAcebac1 (Geneva Biotech). ORF sequences are shown in Supplementary Table S1. Deletion mutants of XKid were generated by PCR-based mutagenesis. For this purpose, primers were designed through the QuickChange Primer Design tool, a web-based application (Agilent). PCR-based mutagenesis was performed using KOD plus neo DNA polymerase (TOYOBO).

Expression of XKid and Kid in Sf9 cells

Sf9 cells (Thermo Fisher Scientific) were maintained in Sf900^{TM} II SFM (Thermo Fisher Scientific) at 27°C. DH10Bac (Thermo Fisher Scientific) were transformed to generate bacmid. To prepare baculovirus, 1×10^6 cells of Sf9 cells were transferred to each well of a tissue-culture treated 6 well plate. After the cells attached to the bottom of the dishes, about ~5 μg of bacmid were transfected using 5 μL of TransIT®-Insect transfection reagent (Takara Bio Inc.). 5 days after initial transfection, the culture media were collected and spun at 3,000 × g for 3 min to obtain the supernatant (P1). For protein expression, 400 mL of Sf9 cells (2×10^6 cells/mL) were infected with 200 μL of P1 virus and cultured for 65 h at 27°C. Cells were harvested and stocked at -80°C.

Purification of proteins

We failed to purify hKid-EGFP and hKid-superfolder GFP due to the insolubility. In contrast, mNeonGreen fusion and mStayGold fusion stabilized hKid and enabled purification.

Sf9 cells were resuspended in 40 mL of Kid lysis buffer (50 mM HEPES-KOH, pH 7.5, 500 mM KCH3COO, 2 mM MgSO4, 1 mM EGTA, 10% glycerol) along with 1 mM DTT, 1 mM PMSF, 0.1 mM ATP and 0.5% Triton X-100. After incubating on ice for 10 min, lysates were cleared by centrifugation (100,000 × g, 20 min, 4°C) and subjected to affinity chromatography. Lysate was loaded on Streptactin-XT resin (IBA Lifesciences, Göttingen, Germany) (bead volume: 2 ml). The resin was washed with 40 ml Kid wash buffer (50 mM HEPES-KOH, pH 8.0, 500 mM KCH_3COO, 2 mM $MgSO_4$, 1 mM EGTA, 10% glycerol). Protein was eluted with 40 ml Kid elution buffer (50 mM HEPES-KOH, pH 8.0, 500 mM KCH_3COO, 2 mM $MgSO_4$, 1 mM EGTA, 10% glycerol, 200 mM biotin). Eluted solution was concentrated using an Amicon Ultra 15 (Merck) and then separated on an NGC chromatography system (Bio-Rad) equipped with a Superdex 200 Increase 10/300 GL column (Cytiva). Peak fractions were collected and concentrated using an Amicon Ultra 4 (Merck). Proteins were analyzed by SDS-PAGE using TGX Stain-Free gel (Bio-Rad). Concentrated proteins were aliquoted and snap-frozen in liquid nitrogen.

Mass photometry

Purified hKid and XKid obtained from the peak fractions in the SEC analysis were pooled, snap-frozen and stored until measurement. Prior to measurement, the proteins were thawed and diluted to a final concentration 5 - 10 nM in GF150 buffer (25 mM HEPES, 150 mM KCl, 2 mM $MgCl_2$, pH 7.2). Mass photometry was performed using a Refeyn OneMP mass photometer (Refeyn) and Refeyn AcquireMP version 2.3 software, with default parameters set by Refeyn AcquireMP. Bovine serum albumin (BSA) was used as a control to determine the molecular weight. The results were subsequently analyzed and graphs were prepared to visualize the data using Refeyn DiscoverMP version 2.3.

Preparation of microtubules

Tubulin was purified from porcine brain as described (Castoldi and Popov, 2003). Tubulin was labeled with Biotin-PEG_2-NHS ester (Tokyo Chemical Industry, Tokyo, Japan) and AZDye647 NHS ester (Fluoroprobes, Scottsdale, AZ, USA) as described (Al-Bassam, 2014). To polymerize Taxol-stabilized microtubules labeled with biotin and AZDye647, 30 µM unlabeled tubulin, 1.5 µM biotin-labeled tubulin and 1.5 µM AZDye647-labeled tubulin were mixed in BRB80 buffer supplemented with 1 mM GTP and incubated for 15 min at 37°C. Then, an equal amount of BRB80 supplemented with 40 µM taxol was added and further incubated for more than 15 min. The solution was loaded on BRB80 supplemented with 300 mM sucrose and 20 µM taxol and ultracentrifuged at 100,000 g for 5 min at 30°C. The pellet was resuspended in BRB80 supplemented with 20 µM taxol.

Preparation of fluorescent-labelled DNA for the TIRF assay

To prepare 100 bp DNA fragment, oligonucleotides labelled with Cy3 were purchased from Integrated DNA Technologies, Inc. (Coralville, Iowa, USA). Following oligonucleotides were synthesized; Cy3-5'-GAGAATCGCCGGTTGATAATCTTCCTAGTAGGTAGTATTGGTGTTGAGTCGCTCA-3' (Oligonucleotide #1) Cy3-5'-GAGAATCGCCGGTTGATAATCTTTGAGCGACTCAACACCAATACTACCTACTAGG- 3' (Oligonucleotide #2) Underlines indicate sequences that form double-stranded DNA.

Double-stranded DNA was prepared using either a VeritiPro Thermal Cycler (Applied Biosystems) or a C1000 Touch Thermal Cycler (Bio-Rad). 1 µM of Oligonucleotides #1 and #2 were mixed and subjected to the following protocol: an initial incubation at 96 °C for 2 minutes, followed by incubation at 25 °C for 1 minutes, and subsequently to 4 °C. For single-stranded DNA preparation, Oligonucleotide #1 was incubated at 96 °C and then cooled to 4 °C.

To prepare 1000-bp and 2000-bp DNAfragments, Cy3-labeled oligonucleotides were purchased from Eurofins Genomics K.K. (Tokyo, Japan). The following oligonucleotides were synthesized: Cy3-5'-TGATGACGGTGAAAACCTCTGACAC-3' (pUC19_F) 5'-TATGAGAAAGCGCCACGCTTCCCG-3' (pUC19_R_1000bp) 5'-GATCGGAGGACCGAAGGAGCTAACC-3'(pUC19_R_2000bp) PCR was performed using pUC19 as the template and KOD FX Neo DNA polymerase. After agarose gel electrophoresis, the 1,000-bp and 2,000-bp DNA fragments were purified.

Double-stranded and single-strand DNA were prepared on the day of the experiment, immediately before the TIRF single-molecule motility assays. Old DNA can potentially cause high background.

TIRF single-molecule motility assays

Purified Kid proteins described above were thawed and analyzed. KIF1A (1-393)LZ, that was described in our previous work (Anazawa et al., 2022), was also thawed and reanalyzed. TIRF assays using porcine microtubules were performed as described (Chiba et al., 2019). Glass chambers were prepared by acid washing as previously described (Chiba et al., 2022). Glass chambers were coated with PLL-PEG-biotin (50% labelled, SuSoS, Dübendorf, Switzerland) and streptavidin (Wako). Polymerized microtubules were flowed into flow chambers and allowed to adhere for 5–10 min. Unbound microtubules were washed away using assay buffer (90 mM HEPES-KOH pH 7.4, 50 mM KCH_3COO, 2 mM $Mg(CH_3COO)_2$, 1 mM EGTA, 10% glycerol, 0.1 mg/ml biotin–BSA, 0.2 mg/ml kappa-casein, 0.5% Pluronic F127, 2 mM ATP, and an oxygen scavenging system composed of PCA/PCD/Trolox). Purified Kid was diluted to indicated concentrations in the assay buffer. Then, the solution was flowed into the glass chamber. An ECLIPSE Ti2-E microscope equipped with a CFI Apochromat TIRF 100XC Oil objective lens (1.49 NA), an Andor iXion life 897 camera and a Ti2-LAPP illumination system (Nikon, Tokyo, Japan) was used to observe the motility. NIS-Elements AR software ver. 5.2 (Nikon) was used to control the system. At least three independent experiments were conducted for each measurement.

MSD analysis

Single-particle trajectories of fluorescent XKid(1-496) and XKid(1-437) molecules were obtained by manually tracking fluorescent puncta in kymographs. For each trajectory, the MSD was calculated for each lag time, Δt, as:

$$\mathrm{MSD}(\Delta t) = \left\langle [x(t+\Delta t) - x(t)]^2 \right\rangle ,$$

where x(t) is the one-dimensional position of the particle along the microtubule or DNA axis, and the brackets denote averaging over all displacement pairs with the same lag time. When the time intervals between tracked points were not strictly uniform, Δt was defined as the mean time difference of all displacement pairs contributing to that lag. The standard error of the MSD for each lag time was calculated as SD/√N, where N is the number of displacement pairs. To minimize the influence of reduced sampling at longer lag times and end-point effects, curve fitting was restricted to the initial region of each MSD curve. Unless otherwise indicated, lag times within approximately the first 60% of the total trajectory duration were used. Lag times were included in the fitting only when they were calculated from at least 10 displacement pairs. Each MSD curve was fitted to the power-law relationship:

$$\mathrm{MSD} = A(\Delta t)^{\alpha},$$

where A is a scaling coefficient and α is the anomalous diffusion exponent.

Alphafold2 analysis

Alphafold2 analysis was conducted on Google Colaboratory (Jumper et al., 2021; Mirdita et al., 2022). We analyzed the amino acid sequences of KIF5C, XKid, and hKid, ranging from the neck linker to the end of coiled-coil 1. The sequences are detailed in Supplementary Table S2. The analysis was based on the assumption that these fragments form dimers and XKid and hKid fold in the similar manner.

Alphafold3 analysis

Alphafold3 analysis was conducted on Alphafold Server (*https://alphafoldserver.com/*). We analyzed the amino acid sequences of the DNA binding domain of XKid and 15-bp dsDNA. The sequences are detailed in Supplementary Table S3.

Statistical analyses and graph preparation

Statistical analyses and graph preparation were conducted using GraphPad Prism version 10. Details on the statistical methods are provided in the figure legends. Graphs were created with GraphPad Prism version 10, exported in PDF format, and aligned using Adobe Illustrator 2023.

Data availability

Figure 1-source data 1 and 2, Figure 3-source data 1, Figure 5-source data 1 and 2, Figure 6-source data 1, 2 and 3 contain the numerical data used to generate the figures.

Acknowledgements

We would like to thank the members of Niwa lab for useful discussions. We also would like to thank Dr. Atsushi Nakagawa and Mr. Jiye Wang (Osaka University) for technical assistance. SN was supported by JSPS KAKENHI (grant no. JP23H02472). TK was supported by JSPS KAKENHI (grant no. JP23KJ0168). KC was supported by JSPS KAKENHI (grant no. JP22K15053), Uehara Memorial Foundation, Naito Foundation and MEXT Leading Initiative for Excellent Researchers (grant no. JPMXS0320200156). This work was performed under the Collaborative Research Program of Institute for Protein Research, Osaka University, CR-24-02.

Additional information

Author contributions

Shinsuke Niwa: Conceptualization; Resources; Data curation; Formal analysis; Project administration; Supervision; Funding acquisition; Validation; Investigation; Visualization; Methodology; Writing—original draft; Writing—review and editing.

Natsuki Furusaki: Resources; Data curation; Formal analysis; Validation; Investigation

Tomoki Kita: Resources; Data curation; Formal analysis; Validation; Investigation

Kyoko Chiba: Resources; Data curation; Formal analysis; Supervision; Funding acquisition; Project administration; Writing—review and editing.

Statement

During the preparation of this work the authors used GPT4.0 in order to check English grammar and improve English writing. After using this tool, the authors reviewed and edited the content as needed and take full responsibility for the content of the publication.

Funding

Funder	Grant reference number	Author
Japan Society for the Promotion of Science (JSPS)	JP23H02472	Shinsuke Niwa
Japan Society for the Promotion of Science (JSPS)	JP23KJ0168	Tomoki Kita
Japan Society for the Promotion of Science (JSPS)	JP22K15053	Kyoko Chiba
Uehara Memorial Foundation (UMF)		Kyoko Chiba
Naito Foundation (内藤記念科学振興財団)		Kyoko Chiba
Takeda Science Foundation (TSF)	2024036450	Kyoko Chiba
Astellas Foundation for Research on Metabolic Disorders (AFRMD)	2024a1048	Kyoko Chiba

Author ORCID iDs

Shinsuke Niwa: https://orcid.org/0000-0002-8367-9228

Additional files

Movie S1. The motility of XKid was analyzed through time-lapse imaging recorded at 0.5 frames per second (fps) and played back at 25 fps. The dimensions of the displayed frame are 30 μm by 7 μm.

Movie S2. The motility of hKid was analyzed through time-lapse imaging recorded at 0.5 fps and played back at 25 fps. The dimensions of the displayed frame are 30 μm by 7 μm.

Movie S3. The motility of KIF1AMD-XKidSt was analyzed through time-lapse imaging recorded at 10 fps and played back at 25 fps. The dimensions of the displayed frame are 30 μm by 7 μm.

Movie S4. The motility of KIF1A(1-393)LZ was analyzed through time-lapse imaging recorded at 10 fps and played back at 25 fps. The dimensions of the displayed frame are 30 μm by 7 μm.

Movie S5. The motility of hKid-mNeonGreen (Green) and Cy3 labelled double-strand DNA (Red) was observed through time-lapse imaging recorded at 0.5 fps and played back at 10 fps. The dimensions of the displayed frame are 25 μm by 8 μm.

Supplemental Figures

Table S1
Table S2
Table S3

References

1. **Afshar K.,** Barton N.R., Hawley R.S., Goldstein L.S. (1995) DNA binding and meiotic chromosomal localization of the Drosophila nod kinesin-like protein. *Cell* **81**:129-138 https://doi.org/10.1016/0092-8674(95)90377-1 | PubMed
2. **Al-Bassam J** (2014) Reconstituting Dynamic Microtubule Polymerization Regulation by TOG Domain Proteins. *Methods in Enzymology* **540**:131-148 https://doi.org/10.1016/b978-0-12-397924-7.00008-x | PubMed
3. **Anazawa Y.,** Kita T., Iguchi R., Hayashi K., Niwa S. (2022) De novo mutations in KIF1A-associated neuronal disorder (KAND) dominant-negatively inhibit motor activity and axonal transport of synaptic vesicle precursors. *Proc Natl Acad Sci U S A* **119**:e2113795119 https://doi.org/10.1073/pnas.2113795119 | PubMed
4. **Antonio C.,** Ferby I., Wilhelm H., Jones M., Karsenti E., Nebreda A.R., Vernos I. (2000) Xkid, a chromokinesin required for chromosome alignment on the metaphase plate. *Cell* **102**:425-435 https://doi.org/10.1016/s0092-8674(00)00048-9 | PubMed
5. **Bieling P.,** Kronja I., Surrey T. (2010) Microtubule motility on reconstituted meiotic chromatin. *Curr Biol* **20**:763-769 https://doi.org/10.1016/j.cub.2010.02.067 | PubMed
6. **Brouhard G.J.,** Hunt A.J. (2005) Microtubule movements on the arms of mitotic chromosomes: polar ejection forces quantified in vitro. *Proc Natl Acad Sci U S A* **102**:13903-13908 https://doi.org/10.1073/pnas.0506017102 | PubMed
7. **Case R.B.,** Rice S., Hart C.L., Ly B., Vale R.D. (2000) Role of the kinesin neck linker and catalytic core in microtubule-based motility. *Curr Biol* **10**:157-160 https://doi.org/10.1016/s0960-9822(00)00316-x | PubMed
8. **Castoldi M.,** Popov A.V. (2003) Purification of brain tubulin through two cycles of polymerization-depolymerization in a high-molarity buffer. *Protein Expr Purif* **32**:83-88 https://doi.org/10.1016/s1046-5928(03)00218-3 | PubMed
9. **Chiba K.,** Kita T., Anazawa Y., Niwa S. (2023) Insight into the regulation of axonal transport from the study of KIF1A-associated neurological disorder. *J Cell Sci* **136** https://doi.org/10.1242/jcs.260742 | PubMed
10. **Chiba K.,** Niwa S. (2024) Autoinhibition and activation of kinesin-1 and their involvement in amyotrophic lateral sclerosis. *Curr Opin Cell Biol* **86**:102301 https://doi.org/10.1016/j.ceb.2023.102301 | PubMed
11. **Chiba K.,** Ori-McKenney K.M., Niwa S., McKenney R.J. (2022) Synergistic autoinhibition and activation mechanisms control kinesin-1 motor activity. *Cell Rep* **39**:110900 https://doi.org/10.1016/j.celrep.2022.110900 | PubMed
12. **Chiba K.,** Takahashi H., Chen M., Obinata H., Arai S., Hashimoto K., Oda T., McKenney R.J., Niwa S. (2019) Disease-associated mutations hyperactivate KIF1A motility and anterograde axonal transport of synaptic vesicle precursors. *Proc Natl Acad Sci U S A* **116**:18429-18434 https://doi.org/10.1073/pnas.1905690116 | PubMed
13. **Doherty A.J.,** Serpell L.C., Ponting C.P. (1996) The helix-hairpin-helix DNA-binding motif: a structural basis for non-sequence-specific recognition of DNA. *Nucleic Acids Res* **24**:2488-2497 https://doi.org/10.1093/nar/24.13.2488 | PubMed
14. **Fan X.M. R.J.** (2022) Control of motor landing and processivity by the CAP-Gly domain in the KIF13B tail. *Nat Commun* **14**:4715 https://doi.org/10.1038/s41467-023-40425-4 | PubMed

15. **Funabiki H.,** Murray A.W. (2000) The Xenopus chromokinesin Xkid is essential for metaphase chromosome alignment and must be degraded to allow anaphase chromosome movement. *Cell* **102**:411-424 https://doi.org/10.1016/s0092-8674(00)00047-7 | PubMed

16. **Gibson D.G.,** Young L., Chuang R.Y., Venter J.C., Hutchison C.A., Smith H.O. (2009) Enzymatic assembly of DNA molecules up to several hundred kilobases. *Nat Methods* **6**:343-345 https://doi.org/10.1038/nmeth.1318 | PubMed

17. **Hackney D.D** (1995) Highly processive microtubule-stimulated ATP hydrolysis by dimeric kinesin head domains. *Nature* **377**:448-450 https://doi.org/10.1038/377448a0 | PubMed

18. **Hancock W.O.,** Howard J. (1998) Processivity of the motor protein kinesin requires two heads. *J Cell Biol* **140**:1395-1405 https://doi.org/10.1083/jcb.140.6.1395 | PubMed

19. **Hoeprich G.J.,** Thompson A.R., McVicker D.P., Hancock W.O., Berger C.L. (2014) Kinesin's neck-linker determines its ability to navigate obstacles on the microtubule surface. *Biophys J* **106**:1691-1700 https://doi.org/10.1016/j.bpj.2014.02.034 | PubMed

20. **Iemura K.,** Tanaka K. (2015) Chromokinesin Kid and kinetochore kinesin CENP-E differentially support chromosome congression without end-on attachment to microtubules. *Nat Commun* **6**:6447 https://doi.org/10.1038/ncomms7447 | PubMed

21. **Isojima H.,** Mori T., Tomishige M. (2010) Optimal Size of the Neck Linker is Important for the Coordinated Processive Movement of Kinesin-1. *Biophysical Journal* **98**:369a-369a https://doi.org/10.1016/j.bpj.2009.12.1995

22. **Jumper J.,** Evans R., Pritzel A., Green T., Figurnov M., Ronneberger O., Tunyasuvunakool K., Bates R., Zidek A., Potapenko A., *et al.* (2021) Highly accurate protein structure prediction with AlphaFold. *Nature* **596**:583-589 https://doi.org/10.1038/s41586-021-03819-2 | PubMed

23. **Kita T.,** Chiba K., Wang J., Nakagawa A., Niwa S. (2024) Comparative analysis of two Caenorhabditis elegans kinesins KLP-6 and UNC-104 reveals a common and distinct activation mechanism in kinesin-3. *eLife* **12** https://doi.org/10.7554/elife.89040 | PubMed

24. **Levesque A.A.,** Compton D.A. (2001) The chromokinesin Kid is necessary for chromosome arm orientation and oscillation, but not congression, on mitotic spindles. *J Cell Biol* **154**:1135-1146 https://doi.org/10.1083/jcb.200106093 | PubMed

25. **Li C.,** Xue C., Yang Q., Low B.C., Liou Y.C. (2016) NuSAP governs chromosome oscillation by facilitating the Kid-generated polar ejection force. *Nat Commun* **7**:10597 https://doi.org/10.1038/ncomms10597 | PubMed

26. **Malaby H.L.,** Lessard D.V., Berger C.L., Stumpff J. (2019) KIF18A's neck linker permits navigation of microtubule-bound obstacles within the mitotic spindle. *Life Sci Alliance* **2** https://doi.org/10.26508/lsa.201800169 | PubMed

27. **Matthies H.J.,** Baskin R.J., Hawley R.S. (2001) Orphan kinesin NOD lacks motile properties but does possess a microtubule-stimulated ATPase activity. *Mol Biol Cell* **12**:4000-4012 https://doi.org/10.1091/mbc.12.12.4000 | PubMed

28. **Mirdita M.,** Schutze K., Moriwaki Y., Heo L., Ovchinnikov S., Steinegger M. (2022) ColabFold: making protein folding accessible to all. *Nat Methods* **19**:679-682 https://doi.org/10.1038/s41592-022-01488-1 | PubMed

29. **Ohsugi M.,** Tokai-Nishizumi N., Shiroguchi K., Toyoshima Y.Y., Inoue J., Yamamoto T. (2003) Cdc2-mediated phosphorylation of Kid controls its distribution to spindle and chromosomes. *EMBO J* **22**:2091-2103 https://doi.org/10.1093/emboj/cdg208 | PubMed

30. **Okada Y.,** Higuchi H., Hirokawa N. (2003) Processivity of the single-headed kinesin KIF1A through biased binding to tubulin. *Nature* **424**:574-577 https://doi.org/10.1038/nature01804 | PubMed

31. **Pike R.,** Ortiz-Zapater E., Lumicisi B., Santis G., Parsons M. (2018) KIF22 coordinates CAR and EGFR dynamics to promote cancer cell proliferation. *Sci Signal* **11** https://doi.org/10.1126/scisignal.aaq1060 | PubMed

32. **Rieder C.L.,** Davison E.A., Jensen L.C., Cassimeris L., Salmon E.D. (1986) Oscillatory movements of monooriented chromosomes and their position relative to the spindle pole result from the ejection properties of the aster and half-spindle. *J Cell Biol* **103**:581-591 https://doi.org/10.1083/jcb.103.2.581 | PubMed

33. **Shastry S.,** Hancock W.O. (2010) Neck linker length determines the degree of processivity in kinesin-1 and kinesin-2 motors. *Curr Biol* **20**:939-943 https://doi.org/10.1016/j.cub.2010.03.065 | PubMed

34. **Shastry S.,** Hancock W.O. (2011) Interhead tension determines processivity across diverse N-terminal kinesins. *Proc Natl Acad Sci U S A* **108**:16253-16258 https://doi.org/10.1073/pnas.1102628108 | PubMed

35. **Shiroguchi K.,** Ohsugi M., Edamatsu M., Yamamoto T., Toyoshima Y.Y. (2003) The second microtubule-binding site of monomeric kid enhances the microtubule affinity. *J Biol Chem* **278**:22460-22465 https://doi.org/10.1074/jbc.m212274200 | PubMed

36. **Soeda S.,** Yamada-Nomoto K., Ohsugi M. (2016) The microtubule-binding and coiled-coil domains of Kid are required to turn off the polar ejection force at anaphase. *J Cell Sci* **129**:3609-3619 https://doi.org/10.1242/jcs.189969 | PubMed

37. **Sonn-Segev A.,** Belacic K., Bodrug T., Young G., VanderLinden R.T., Schulman B.A., Schimpf J., Friedrich T., Dip P.V., Schwartz T.U., *et al.* (2020) Quantifying the heterogeneity of macromolecular machines by mass photometry. *Nat Commun* **11**:1772 https://doi.org/10.1038/s41467-020-15642-w | PubMed

38. **Soppina V.,** Norris S.R., Dizaji A.S., Kortus M., Veatch S., Peckham M., Verhey K.J. (2014) Dimerization of mammalian kinesin-3 motors results in superprocessive motion. *Proc Natl Acad Sci U S A* **111**:5562-5567 https://doi.org/10.1073/pnas.1400759111 | PubMed

39. **Stumpff J.,** Wagenbach M., Franck A., Asbury C.L., Wordeman L. (2012) Kif18A and chromokinesins confine centromere movements via microtubule growth suppression and spatial control of kinetochore tension. *Dev Cell* **22**:1017-1029 https://doi.org/10.1016/j.devcel.2012.02.013 | PubMed

40. **Takagi J.,** Itabashi T., Suzuki K., Ishiwata S. (2013) Chromosome position at the spindle equator is regulated by chromokinesin and a bipolar microtubule array. *Sci Rep* **3**:2808 https://doi.org/10.1038/srep02808 | PubMed

41. **Tan Z.,** Yue Y., da Veiga Leprevost F., Haynes S.E., Basrur V., Nesvizhskii A.I., Verhey K.J., Cianfrocco M.A. (2023) Autoinhibited kinesin-1 adopts a hierarchical folding pattern. *eLife* **12**:RP86776 https://doi.org/10.7554/elife.86776 | PubMed

42. **Thompson A.F.,** Blackburn P.R., Arons N.S., Stevens S.N., Babovic-Vuksanovic D., Lian J.B., Klee E.W., Stumpff J. (2022) Pathogenic mutations in the chromokinesin KIF22 disrupt anaphase chromosome segregation. *eLife* **11** https://doi.org/10.7554/elife.78653 | PubMed

43. **Tokai N.,** Fujimoto-Nishiyama A., Toyoshima Y., Yonemura S., Tsukita S., Inoue J., Yamamota T. (1996) Kid, a novel kinesin-like DNA binding protein, is localized to chromosomes and the mitotic spindle. *EMBO J* **15**:457-467 https://doi.org/10.1002/j.1460-2075.1996.tb00378.x | PubMed

44. **Tomishige M.,** Klopfenstein D.R., Vale R.D. (2002) Conversion of Unc104/KIF1A kinesin into a processive motor after dimerization. *Science* **297**:2263-2267 https://doi.org/10.1126/science.1073386 | PubMed

45. **Walker B.C.,** Tempel W., Zhu H., Park H., Cochran J.C. (2019) Chromokinesins NOD and KID Use Distinct ATPase Mechanisms and Microtubule Interactions To Perform a Similar Function. *Biochemistry* **58**:2326-2338 https://doi.org/10.1021/acs.biochem.9b00011 | PubMed

46. **Wandke C.,** Barisic M., Sigl R., Rauch V., Wolf F., Amaro A.C., Tan C.H., Pereira A.J., Kutay U., Maiato H., *et al.* (2012) Human chromokinesins promote chromosome congression and spindle microtubule dynamics during mitosis. *J Cell Biol* **198**:847-863 https://doi.org/10.1083/jcb.201110060 | PubMed

47. **Wang W.,** Ren J., Song W., Zhang Y., Feng W. (2022) The architecture of kinesin-3 KLP-6 reveals a multilevel-lockdown mechanism for autoinhibition. *Nat Commun* **13**:4281 https://doi.org/10.1038/s41467-022-32048-y | PubMed

48. **Weijman J.F.,** Yadav S.K.N., Surridge K.J., Cross J.A., Borucu U., Mantell J., Woolfson D.N., Schaffitzel C., Dodding M.P. (2022) Molecular architecture of the autoinhibited kinesin-1 lambda particle. *Sci Adv* **8**:eabp9660 https://doi.org/10.1126/sciadv.abp9660 | PubMed

49. **Wordeman L** (2010) How kinesin motor proteins drive mitotic spindle function: Lessons from molecular assays. *Semin Cell Dev Biol* **21**:260-268 https://doi.org/10.1016/j.semcdb.2010.01.018 | PubMed

50. **Yajima J.,** Edamatsu M., Watai-Nishii J., Tokai-Nishizumi N., Yamamoto T., Toyoshima Y.Y. (2003) The human chromokinesin Kid is a plus end-directed microtubule-based motor. *EMBO J* **22**:1067-1074 https://doi.org/10.1093/emboj/cdg102 | PubMed

51. **Ye A.A.,** Verma V., Maresca T.J. (2018) NOD is a plus end-directed motor that binds EB1 via a new microtubule tip localization sequence. *J Cell Biol* **217**:3007-3017 https://doi.org/10.1083/jcb.201708109 | PubMed

52. **Yildiz A.,** Tomishige M., Gennerich A., Vale R.D. (2008) Intramolecular strain coordinates kinesin stepping behavior along microtubules. *Cell* **134**:1030-1041 https://doi.org/10.1016/j.cell.2008.07.018 | PubMed

Peer reviews

Reviewer #1 (Public review):

[Editors' note: this version has been assessed by the Reviewing Editor without further input from the original reviewers. The authors have addressed the comments raised in the previous round of review.]

Summary:

Mitotic kinesins carry out crucial roles in intracellular motility and mitotic spindle organization. Although many mitotic kinesins have been extensively studied, a few conserved mitotic motors remain poorly explored, including chromosome-associated kinesins. Here, Furusaki et al reconstitute recombinant chromosome-associated kinesin or chromokinesin (Kid) and reveal processive plus-end motility along microtubules. The authors purify multiple versions of Kid, revealing dimeric organization and their processive microtubule plus-ended motility which depends on their conserved motor domains, neck linkers, and coiled-coil regions. The study reveals for the first time that KID can recruit and transport duplex DNA along microtubules using its conserved C-terminal DNA binding domain. The work provides crucial revised thinking about the mechanisms of Chromokinesins mitosis as physical processive motors that mobilize chromosomes towards the microtubule plus ends in early metaphase.

Strengths:

The authors reconstitute multiple chromosome-associated kinesin (KID) orthologs from Xenopus and humans with microtubules and determine their oligomerization. The study shows how coiled-coil and neck linker regions of KID are essential for its function as its deletion leads to non-processive motility. Chimeras placing the KID coiled-coil and neck linker on the KIF1A motor domain led to the production of a processive recombinant motor supporting the compatibility of their motility mechanisms. The KID c-terminal tail binds and transports only double-stranded DNA and its deletion or single-stranded DNA leads to defects in this activity.

https://doi.org/10.7554/eLife.102828.2.sa2

Reviewer #2 (Public review):

Summary:

Previous work in the field highlighted the role of the kinesin-10 motor protein Kid (KIF22) in the polar ejection force during prometaphase. However, the biochemical and biophysical properties of Kid that enabled it to serve in this role were unclear. The authors demonstrate that human and xenopus Kid proteins are processive kinesins that function as homodimeric molecules. The data are solid and support the findings although the text could use some editing to improve clarity.

Strengths:

A highlight of the work is the reconstitution of DNA transport in vitro.

A second highlight is the demonstration that the monomer vs dimer state is dependent on protein concentration.

https://doi.org/10.7554/eLife.102828.2.sa1

Author response:

The following is the authors' response to the original reviews.

In this revised manuscript, we added new analyses of the DNA-binding tail domain of Kid. AlphaFold 3 predictions suggested that dimeric Kid interacts more stably with double-stranded DNA than monomeric Kid. To experimentally test this prediction, we introduced a point mutation into a critical residue predicted to contribute to DNA binding. Consistent with the AlphaFold 3 model, this mutation abolished the interaction between Kid and DNA.

We also extended our DNA transport assays by testing DNA substrates of different lengths. In addition to 100-bp double-stranded DNA, full-length Kid transported 1,000-bp and 2,000-bp DNA molecules along microtubules *in vitro*. These findings show that Kid can transport longer duplex DNA substrates than those initially tested, although these substrates do not fully recapitulate the organization of condensed chromatin.

Furthermore, we performed dual-color imaging using independently purified Kid-mScarlet3 and Kid-mStayGold proteins. We consistently observed co-migration of the two fluorescently labeled Kid molecules along microtubules, supporting the conclusion that Kid forms dimers on microtubules.

> ***Public Reviews:***
>
> ***Reviewer #1 (Public review):***
>
> *Summary:*
>
> *Mitotic kinesins carry out crucial roles in intracellular motility and mitotic spindle organization. Although many mitotic kinesins have been extensively studied, a few conserved mitotic motors remain poorly explored, including chromosome-associated kinesins. Here, Furusaki et al reconstitute recombinant chromosome-associated kinesin or chromokinesin (Kid) and reveal processive plus-end motility along microtubules. The authors purify multiple versions of Kid, revealing dimeric organization and their processive microtubule plus-ended motility which depends on their conserved motor domains, neck linkers, and coiled-coil regions. The study reveals for the first time that KID can recruit and transport duplex DNA along microtubules using its conserved C-terminal DNA binding domain. The work provides crucial revised thinking about the mechanisms*

> *of Chromokinesins mitosis as physical processive motors that mobilize chromosomes towards the microtubule plus ends in early metaphase.*
>
> *Strengths:*
>
> *The authors reconstitute multiple chromosome-associated kinesin (KID) orthologs from Xenopus and humans with microtubules and determine their oligomerization. The study shows how coiled-coil and neck linker regions of KID are essential for its function as its deletion leads to non-processive motility. CHimeras placing the KID coiled-coil and neck linker on the KIF1A motor domain led to the production of a processive recombinant motor supporting the compatibility of their motility mechanisms. The KID c-terminal tail binds and transports only double-stranded DNA and its deletion or single-stranded DNA leads to defects in this activity.*

Thank you very much.

> *Weaknesses:*
>
> *A minor weakness in the studies is that they do not resolve the mechanisms of KID in binding large duplex DNA molecules or condensed chromatin. The authors suggest a model in which KID forms multimers along large chromosomes that lead to their transport, but this model was not directly tested.*

We agree with the reviewer that our study does not directly resolve how Kid binds large duplex DNA molecules or condensed chromatin. In the revised manuscript, we have therefore softened our model and now present the idea that multiple Kid dimers act along chromosomes as a possible mechanism rather than a demonstrated conclusion. To strengthen the mechanistic basis of DNA binding, we added AlphaFold 3-based analysis of the Kid DNA-binding tail domain and experimentally tested a predicted DNA-binding residue. Mutation of this residue abolished Kid–DNA binding, supporting the proposed role of the tail domain in DNA engagement. We also added dual-color imaging experiments showing co-migration of independently purified Kid-mScarlet3 and Kid-mStayGold on microtubules, supporting dimer formation on microtubules. We now explicitly state that future studies using chromatinized DNA or chromosome-like substrates will be required to determine how Kid interacts with condensed chromatin in a cellular context.

> ***Reviewer #2 (Public review):***
>
> *Summary:*
>
> *Previous work in the field highlighted the role of the kinesin-10 motor protein Kid (KIF22) in the polar ejection force during prometaphase. However, the biochemical and biophysical properties of Kid that enabled it to serve in this role were unclear. The authors demonstrate that human and xenopus Kid proteins are processive kinesins that function as homodimeric molecules. The data are solid and support the findings although the text could use some editing to improve clarity.*
>
> *Strengths:*
>
> *A highlight of the work is the reconstitution of DNA transport in vitro.*
>
> *A second highlight is the demonstration that the monomer vs dimer state is dependent on protein concentration.*

Thank you very much.

> *Weaknesses:*

> *The authors make several assumptions of the monomer vs dimer state of various Kid constructs without verifying the protein state using e.g. size exclusion chromatography and/or nanophotometry.*

We newly added mass photometry analysis in Figure 3 and Figure 5.

> *They also make statements about monomer-to-dimer transitions on the microtubule without showing or quantifying the data.*

We performed dual color imaging to show the assembly of Kid monomers on microtubules.

> *The discussion needs to better put the work into context regarding the ability of non-processive motors to work in teams (formerly thought to be the case for Kid) and how their findings on Kid change this prevailing view in the case of polar ejection force.*

We have revised the Discussion to better place our findings in the context of collective motor function and polar ejection force generation. Previous biochemical studies led to the prevailing model that Kid is a monomeric and non-processive chromokinesin. Under this model, sustained chromosome movement would require many Kid monomers distributed along chromosome arms to act collectively. Our findings revise this view. We show that full-length Kid forms homodimers, moves processively along microtubules, and directly transports double-stranded DNA. Thus, the elementary force-generating unit of Kid is unlikely to be a non-processive monomer. Instead, a single Kid dimer may act as a processive DNA-bound motor. In the context of mitotic chromosomes, multiple processive Kid dimers bound along chromosome arms could cooperate to generate chromosome-scale polar ejection forces. We have clarified in the Discussion that our model does not exclude ensemble behavior. Rather, it changes the nature of the proposed ensemble from many non-processive monomers to multiple processive dimers.

> *The authors also do not mention previous work on kinesins with non-conventional neck linker/neck coil regions that have been shown to move processively. Their work on Kid needs to be put into this context.*

We thank the reviewer for this important suggestion. We have revised the Discussion to place Kid in the broader context of processive kinesins with non-conventional neck linker or neck coil regions. We now discuss previous work showing that neck-linker length strongly influences kinesin processivity, and that changes in neck-linker length alter the run length and motility properties of kinesin-1, kinesin-2, and other N-terminal kinesins (Shastry and Hancock, 2010; Shastry and Hancock, 2011).

We also discuss studies showing that longer or non-conventional neck linker regions can provide additional functions beyond supporting processive stepping. For example, kinesin-2 can bypass Tau and other microtubule-bound obstacles by protofilament switching, and the neck linker of the mitotic kinesin KIF18A contributes to obstacle navigation within the mitotic spindle (Hoeprich et al., 2014; Malaby et al., 2019).

In this context, we now emphasize that Kid has an exceptionally long and flexible neck linker, approximately four times longer than that of kinesin-1. Despite this non-canonical architecture, the Kid neck linker and coiled-coil region support processive motility, as shown by the processive movement of the KIF1A–Kid chimera. We therefore propose that Kid represents a non-conventional processive chromokinesin whose extended neck linker may help it move along crowded spindle microtubules while remaining attached to DNA or chromatin. We have also stated that this possibility remains to be tested directly.

> ***Recommendations for the authors:***

> ***Reviewer #1 (Recommendations for the authors):***
>
> *Furusaki et al reconstitute effectively the chromosome-associated kinesin. The studies are well performed and effectively controlled with few minor suggestions*
>
> *The studies generally lack a few minor items that would improve the current work:*
>
> *(1) Alpha fold or coiled-coil predictions of the c-terminal region characterizing its organization or the nature of its interaction site with DNA. These should aid the presentation of the work and help refine the boundaries for coiled coils and the DNA binding domain.*

We thank the reviewer for this helpful suggestion. In the revised manuscript, we added AlphaFold 3-based structural predictions and coiled-coil predictions for the C-terminal region of Kid (Figure 7). These analyses helped define the predicted DNA-binding tail domain more clearly. The AlphaFold 3 model also suggested a potential DNA-interaction surface within the C-terminal DNA-binding region. We have incorporated these predictions into the revised figure and modified the text to clarify the domain organization of Kid.

> *(2) The DNA transport motor activity is quite interesting and extending those studies to cover larger segments of DNA which may bind multiple kid motors would be very interesting.*

We thank the reviewer for this helpful suggestion. In the revised manuscript, we extended our DNA transport assays using longer double-stranded DNA fragments. In addition to the 100-bp DNA substrate, we tested 1,000-bp and 2,000-bp DNA fragments. Full-length Kid was able to transport both 1,000-bp and 2,000-bp double-stranded DNA along microtubules *in vitro*. These new data are now included in Figure 6F–I. Interestingly, the motile parameters of 1,000-bp and 2,000-bp DNA were comparable to those observed with 100-bp DNA. This result suggests that, under our reconstituted assay conditions, increasing DNA length does not substantially enhance the apparent transport velocity or run length. One possible explanation is that the interaction between Kid and naked DNA is relatively weak, and thus only one or a small number of Kid molecules productively engage each DNA molecule during transport. Alternatively, additional Kid molecules bound to longer DNA may not strongly affect the measured motility parameters under these assay conditions.

We have added this point to the revised manuscript and now discuss that, in cells, additional factors such as chromatin proteins or chromosome-associated proteins may enhance the avidity or organization of Kid on chromosomes. Future studies using chromatinized DNA or chromosome-like substrates will be needed to determine how multiple Kid molecules engage large chromatin substrates during chromosome congression.

> *(3) The final model regarding KID transporting chromosomes is probably oversimplified since there are few experiments with large stretches of DNA or chromatin that were not conducted. I suggest longer segments of DNA be studied or the model be redrawn to scale.*

We thank the reviewer for this important comment. We agree that the original model was oversimplified because naked DNA fragments do not fully recapitulate the size, structure, or mechanical properties of condensed chromatin or mitotic chromosomes. To address this concern experimentally, we extended our DNA transport assays to longer double-stranded DNA fragments. In addition to 100-bp DNA, we tested 1,000-bp and 2,000-bp DNA fragments and found that full-length hKid can transport both substrates along microtubules *in vitro*. These new data are now included in Figure 6F–I.

However, we agree that these DNA substrates are still much simpler than condensed chromatin. We have therefore revised the final model to avoid implying that the transport of naked DNA fully explains chromosome-scale movement. The revised model now emphasizes that Kid dimers can directly couple DNA to microtubule-based motility, and that multiple Kid dimers may cooperate on chromosome arms to generate polar ejection forces. We state "This model is not drawn to scale and does not fully represent the structural complexity of condensed chromatin." in the revised legends.

We also state explicitly in the Discussion that future experiments using chromatinized DNA or reconstituted chromosome-like substrates will be required to determine how Kid engages condensed chromatin and generates chromosome-scale forces.

> ***Reviewer #2 (Recommendations for the authors):***
>
> *Major points:*
>
> *(1) The authors state that XKid(1-437), which lacks the coiled-coil domain, did not show any processive runs yet Figure 3D does show short events that look like directed movement. They do not appear to be diffusive events as they are uni-directional. The authors need to quantify these results (motility, mean square displacement) as they are essential to their arguments about monomer vs dimer state and processive motility.*

We thank the reviewer for pointing this out. We agree that, in the original kymographs acquired at lower temporal resolution, some short XKid(1–437) events could appear as directional movements. To address this concern, we repeated the single-molecule motility assays with improved temporal resolution. In the revised manuscript, the kymographs for XKid(1–437) were generated from data acquired at 100 ms per pixel, instead of 3 s per pixel in the previous version. This higher temporal resolution more clearly shows that XKid(1–437) undergoes short, diffusion-like fluctuations rather than sustained unidirectional processive movement.

We also quantified these trajectories by mean-square displacement analysis. XKid(1–495), which retains the coiled-coil domain, showed superlinear MSD scaling with an α value of approximately 1.6, consistent with persistent, directionally biased movement. In contrast, XKid(1–437), which lacks the coiled-coil domain, showed an α value of approximately 0.8, consistent with hindered or diffusion-like motion rather than sustained processive motility.

We have added these higher-temporal-resolution data and MSD quantification to the revised Figure 3 and revised the text accordingly. We now state that XKid(1–437) lacks sustained processive runs, rather than implying that it shows no movement at all.

> *The authors speculate that the lack of XKid(1-437) processive runs is due to it being unable to form a homodimer. To confirm that the coiled-coil domain is responsible for dimerization, they fuse the coiled-coil to a fluorescent protein. However, the authors should actually show that XKif(1-437) is a monomer by size exclusion chromatography and/or nanophotometry.*

We thank the reviewer for this important suggestion. We agree that directly determining the oligomeric state of XKid(1–437) is essential for interpreting the loss of processive motility. We therefore performed mass photometry to measure the molecular mass of purified XKid(1–437).

The mass photometry analysis showed that XKid(1–437) was predominantly monomeric, with no detectable dimer population under the conditions tested. In contrast, XKid(1–495), which retains the coiled-coil domain, showed a minor dimer population, similar to full-length XKid.

These results support the conclusion that deletion of the coiled-coil domain disrupts Kid dimerization.

Together with the motility assays and MSD analysis, these data indicate that the coiled-coil domain is required for homodimer formation and sustained processive motility of Kid. We have added these mass photometry data to the revised Figure 3 and revised the text accordingly.

> *(2) Likewise, the chimeric protein KIF1AMD-XKidSt shows processive motility (Figure 4), and thus authors conclude that it must be a dimer. This should be verified using size exclusion chromatography and/or nanophotometry.*

We agree that the oligomeric state of KIF1AMD–XKidSt should be directly examined. We therefore performed mass photometry analysis of purified KIF1AMD–XKidSt.

Mass photometry showed that KIF1AMD–XKidSt behaved similarly to full-length XKid and XKid(1–495). Under the nanomolar concentrations used for mass photometry, KIF1AMD–XKidSt was predominantly monomeric but retained a detectable dimer population. This behavior is consistent with our analysis of full-length Kid and XKid(1–495), which form weak, concentration-dependent dimers. These results indicate that the XKid stalk region in the chimera can support dimer formation, although the dimer is weak under dilute solution conditions.

> *(3) Lines 236-239, the authors state "in TIRF-based motility assays, although Kid predominantly dissociates into monomers in solution, its direct interaction with microtubules leads to an increased local concentration of Kid on the microtubule surface. As a result, this would facilitate the formation of Kid dimers on the microtubules, leading to processive motility." This statement implies that monomeric motors diffuse on the microtubule surface until they can associate and begin processive motion. Do the authors see such events (diffuse motion and/or association of single monomers on microtubules and a resulting change to processive motion? The kymograph in Figure 1C shows only static and motile events for XKid but hKid does appear to undergo diffusive motion. What is the percent of static vs diffusive vs processive events and how does this change with increased concentrations of XKid and HKid?*

We thank the reviewer for this important point. We agree that our original statement was too strong, because we did not directly observe monomeric Kid molecules diffusing on microtubules and then associating to initiate processive movement. We have revised the text to clarify that microtubule-dependent dimerization is a model.

To test this model, we performed dual-color imaging using independently purified hKid–mScarlet3 and hKid–mStayGold. These proteins were mixed at 1 pM each, a concentration at which Kid is expected to be predominantly monomeric in solution. We observed co-migration of the two fluorescently labeled Kid proteins along microtubules, supporting the idea that Kid molecules can associate on microtubules and move together.

However, because of the limited temporal resolution of our two-color TIRF system, we could not directly capture the transition from two monomers to a processive dimer on the microtubule surface. We therefore do not quantify the fraction of static, diffusive, and processive events as a function of concentration in this revised manuscript. Instead, we have softened the relevant statement and explicitly note this limitation in the Discussion.

> *(4) Lines 171-172 - optimal length of neck linker for coordination of the two motor domains has only been shown for kinesin-1 and kinesin-2. In contrast, there are a number of kinesins that do not have typical neck linker domains yet can achieve processivity. The authors need to discuss this work and put their results with Kid into this context.*

As described above, we have revised the Discussion to place Kid in the broader context of processive kinesins with non-conventional neck linker or neck coil regions. We now discuss previous work showing that neck-linker length strongly influences kinesin processivity, and that changes in neck-linker length alter the run length and motility properties of kinesins (Shastry and Hancock, 2010; Shastry and Hancock, 2011).

We also discuss studies showing that longer or non-conventional neck linker regions, such as those of kinesin-2 and KIF18, can provide additional functions beyond supporting processive stepping (Hoeprich et al., 2014; Malaby et al., 2019). In this context, we now emphasize that Kid has an exceptionally long and flexible neck linker, approximately four times longer than that of kinesin-1. We described a possibility that the extended neck linker of Kid may help it move along crowded spindle microtubules while remaining attached to DNA or chromatin while this possibility remains to be tested directly.

> *Minor points:*
>
> *(5) Lines 68-69 should note that non-processive motors have been shown to move cargo if they are present in multiple copies of the cargo. This should also be discussed in the Discussion.*

We described it in the revised manuscript:

“Under this model, sustained chromosome movement would require many Kid monomers distributed along chromosome arms to act collectively.”

“This model preserves the likely importance of motor ensembles on large chromatin, but changes the nature of the ensemble from many non-processive monomers to multiple processive dimers.”

> *(6) For Figure 4, does the KIF1AMD-XKidSt chimeric protein contain both the stalk (coiled-coil?) and tail (DNA binding?) regions of XKid or just the stalk as shown in the schematic?*

We included coiled-coil domain only.

> *(7) For Figure 5, please provide a schematic for XKid(delta tail).*

We now added Alphafold 3 data.

> ***Senior Editor:***
>
> *Along the lines of reviewer #2's request to put the results in the context of existing knowledge, please consider whether you want to cite Pike et al. 2018 (https://doi.org/10.1126/scisignal.aaq1060; some evidence for dimerization in Fig. 4) and Walker et al. 2019 (https://pubs.acs.org/doi/10.1021/acs.biochem.9b00011).*

We have cited these papers in the revised manuscript. These are consistent with our finding that Kid can form dimer at higher concentration while dissociate to monomers in lower concentrations.

https://doi.org/10.7554/eLife.102828.2.sa0